Review

Water-Lubricated Photothermal Surfaces for Anti-Icing and Deicing

Chunlei Gao *, Yongzhi Liu, Yongyi Du

Posted Date: 20 April 2026

doi: 10.20944/preprints202604.1367.v1

Keywords: water lubrication; interfacial lubrication; photothermal superwetting surfaces; ice adhesion; solar-thermal conversion

 doi:10.20944/preprints202604.1367.v1

Review

Water-Lubricated Photothermal Surfaces for Anti-Icing and Deicing

Chunlei Gao [1,*], Yongzhi Liu [2], Yongyi Du [3]

[1] School of Mechanical and Electrical Engineering, Taizhou Vocational and Technical College, Taizhou 318000, China

[2] School of Electronic and Information Engineering, Beijing Jiaotong University, Beijing 100044, China

[3] School of Physics, Beijing Institute of Technology, Beijing 100081, China

* Correspondence: gaocl@tzvtc.edu.cn

Abstract

Ice accumulation on critical infrastructure surfaces threatens operational safety in aviation, power transmission, and transportation systems. Conventional anti-icing and deicing strategies, such as chemical deicers and energy-intensive active heating, have inherent drawbacks. These include environmental pollution, high energy consumption, and low efficiency. In recent years, photothermal-responsive superwetting surfaces have attracted widespread attention. They can harvest renewable solar energy and achieve efficient anti-icing and deicing through tailored interfacial wetting properties. This review summarizes photothermal superwetting surfaces based on the "water as a lubricating layer" strategy. This strategy reduces ice adhesion strength and enables low-energy deicing. It works by forming a continuous lubricating film via photothermally induced interfacial meltwater. We discuss photothermal conversion mechanisms and strategies to enhance performance for stable lubricating film formation. We also analyze the stagewise physics of anti-icing and deicing, focusing on the interfacial tribological behavior of the water film. Key engineering challenges are addressed, including mechanical durability and all-weather applicability. Finally, we clarify future research directions for industrial translation. This review aims to provide theoretical insights and technical pathways for developing next-generation anti-icing and deicing surfaces that are efficient, eco-friendly, and sustainable.

Keywords: water lubrication; interfacial lubrication; photothermal superwetting surfaces; ice adhesion; solar-thermal conversion

1. Introduction

Ice accumulation on critical infrastructure surfaces severely threatens the operational safety and reliability of aviation [1,2], power transmission [3,4], and renewable energy generation systems [5,6]. Conventional anti-icing/deicing technologies, including chemical deicers [7], mechanical removal [8,9], and energy-intensive active heating [10], have inherent drawbacks such as environmental pollution, high cost, and low efficiency, thereby driving an urgent need for passive, energy-autonomous, and sustainable ice protection solutions.

As shown in **Figure 1**, superhydrophobic surfaces (SHS) have emerged as a core research direction for passive anti-icing, as they reduce ice adhesion by minimizing solid-liquid contact [11,12]. Their anti-icing performance was first experimentally verified in 2009 [13,14], and subsequent studies have confirmed that rationally designed micro-nano structures can shorten the contact time of supercooled droplets and delay ice nucleation and growth [15–18]. However, conventional SHS are prone to failure under high humidity and extreme supercooling due to the Cassie-to-Wenzel wetting transition, which triggers a sharp rise in ice adhesion [12,19,20]. Moreover, the detachment of low-adhesion ice still relies on unstable external forces such as wind and gravity [21].

 doi:10.20944/preprints202604.1367.v1

Two alternative strategies based on interfacial lubrication have emerged to address these limitations. Slippery liquid-infused porous surfaces (SLIPS) reduce interfacial friction through a continuous lubricant film [22,23]. Low-interfacial-toughness elastomeric coatings, in contrast, promote ice detachment by inhibiting crack propagation [21,24]. However, they face irreversible lubricant depletion and high deicing force requirements, respectively, highlighting the need for a sustainable in situ lubrication strategy.

In parallel, the development of "armored" SHS [25] with exceptional durability provided a stable platform for the functional integration of photothermal materials. The combination of photothermal materials and superwetting surfaces overcomes the limitations of purely passive protection afforded by conventional icephobic surfaces via solar photothermal conversion [26–28].

The core advantage of photothermal superwetting surfaces lies in the reconstruction of the ice-substrate interface through the “water as a lubricating layer” strategy. Under solar irradiation, localized photothermal heating preferentially melts the thin ice layer in contact with the substrate, forming a continuous in situ lubricating film of liquid water. This film transforms high-adhesion solid-solid contact into low-friction solid-liquid-solid interfacial lubrication contact, drastically reducing ice adhesion and enabling gravity-driven passive deicing at sub-zero temperatures [29].

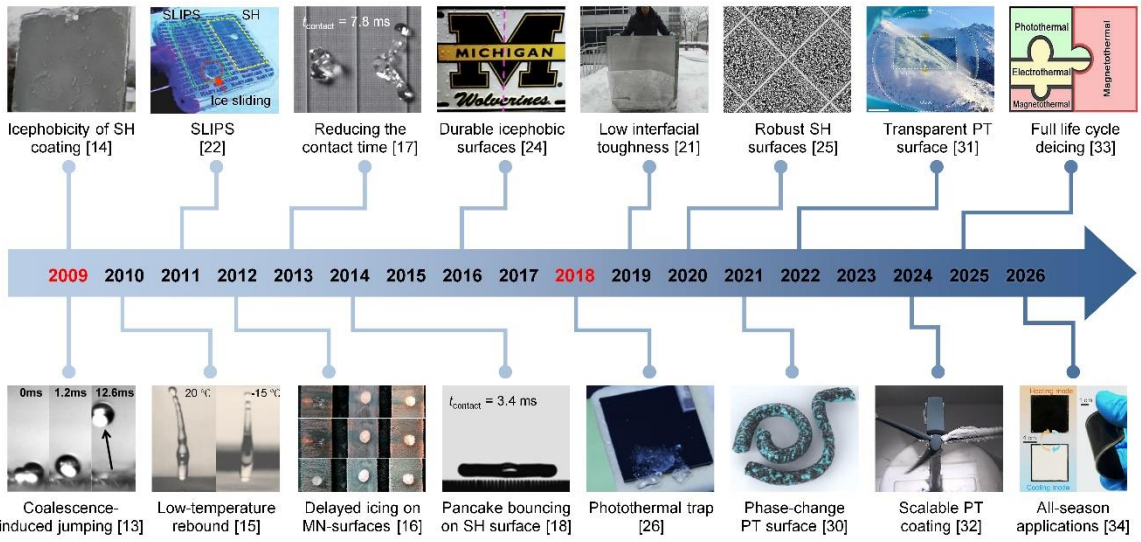

Figure 1. Timeline of key advances in superwetting surfaces for anti-icing and de-icing (2009-2026). Foundational work (2009-2014) established core anti-icing phenomena and droplet dynamics [13–18]. Durability breakthroughs (2011-2019) introduced SLIPS, low-modulus elastomers, and low-interfacial-toughness materials to address structural fragility [21,22,24]. Photothermal-responsive systems (2018-2026) integrate passive anti-icing with active solar-driven de-icing, advancing wear resistance, multi-mode thermal management, and all-season adaptability [25,26,30–34]. All panels reproduced with permission.

This strategy converts meltwater into a lubricating medium, thereby addressing the external-force dependence of SHS and the lubricant depletion of SLIPS. It is widely accepted that interfacial lubrication is the core pathway to ultra-low ice adhesion, but critical gaps remain in the quantitative regulation, long-term stability, and standardized evaluation of the lubricating water film.

This review systematically summarizes research progress on photothermal superwetting anti-icing surfaces based on the water-lubricating film strategy, with a consistent focus on interfacial lubrication behavior. The organization of this review is as follows: Section 2 discusses photothermal conversion mechanisms and material design strategies. Section 3 analyzes the stagewise anti-icing/deicing mechanisms with a focus on interfacial lubrication. Section 4 addresses key engineering challenges. Section 5 outlines future directions.

 doi:10.20944/preprints202604.1367.v1

2. Photothermal Materials for Water-Lubricated Anti-Icing

Photothermal materials are essential for the "water-as-lubricant" anti-icing strategy. Their photothermal efficiency, interfacial heating uniformity, and stability directly govern how quickly, continuously, and reliably a lubricating water film forms at the ice-substrate interface. Localized interfacial heating, not bulk ice melting, is key to forming a continuous water film with minimal energy use [29,35]. This chapter provides a comprehensive review of photothermal mechanisms, major material systems, and design strategies, with an emphasis on how materials engineering enables stable and efficient deicing through the controlled formation of a water film.

2.1. Photothermal Mechanisms and Material Types

For anti-icing and deicing applications involving “water as a lubricating layer”, three mainstream photothermal conversion mechanisms have been developed, categorized by their dominant energy-dissipation pathways and representative material systems. The classification, working principles, and representative material morphologies are summarized in **Figure 2**.

2.1.1. Localized Surface Plasmon Resonance

Localized surface plasmon resonance (LSPR) arises from the collective oscillation of free electrons in nanostructures under light excitation, generating intense, ultrafast, and highly localized interfacial heating (**Figure 2b**) [29]. The fast thermal response and spatial confinement of heat generation inherent to this mechanism avoid the energy waste associated with bulk ice melting, aligning well with the low-energy core requirement of interfacial lubrication. Plasmonic materials used for anti-icing cover a broad compositional spectrum. Noble metals such as Au and Ag were among the first to be explored, but attention has increasingly shifted toward more practical alternatives, copper-based nanomaterials (Cu nanowires, CuS) and refractory transition-metal nitrides, particularly TiN [3,31,36–44].

Noble metal nanostructures (e.g., Au) can achieve near-unity broadband solar absorption through hybrid LSPR modes [31], but their high cost, limited scalability, and insufficient long-term stability restrict engineering deployment. Transition-metal nitride ceramics, particularly titanium nitride (TiN), have emerged as leading alternatives owing to their excellent optical properties, chemical inertness, and mechanical robustness. Superhydrophobic composite coatings employing TiN nanoparticles as the photothermal unit exhibit an 81.9 ℃ temperature rise under 1-sun irradiation while maintaining good wear resistance and stable performance [42]. Achieving uniform dispersion of plasmonic nanoparticles across large areas, however, remains difficult. Non-uniform heating can produce discontinuous water films that locally pin ice and trigger lubrication failure.

2.1.2. Non-Radiative Relaxation

In semiconductor photothermal materials, photon-to-heat conversion proceeds predominantly through non-radiative relaxation (**Figure 2c**). Photoexcited carriers dissipate absorbed photon energy as lattice heat via electron-phonon coupling, thereby avoiding radiative emission losses. The conversion efficiency is intrinsically governed by the material's electronic band structure [45]. Representative semiconductor materials for anti-icing applications include metal oxides (Fe_3O_4), polydopamine (PDA), polyaniline, and polypyrrole (PPy) [28,46–57].

Early anti-icing photothermal coatings employed semiconductor materials such as Fe_3O_4, though few studies elucidated the intrinsic structure-activity relationship between electronic structure and non-radiative decay [28,46,47,49]. A key breakthrough was achieved in titanium suboxide (Ti_xO_{2n-1}) systems. Metallic λ-Ti_3O_5 exhibits a solar absorptivity of 96.4%, owing to nearly dispersionless flat bands induced by Ti-Ti dimers near the Fermi level. These flat bands create a high joint density of states (JDOS), which broadens light absorption and accelerates non-radiative relaxation of hot carriers [58]. Defect engineering must therefore strike a delicate balance: sufficient

 doi:10.20944/preprints202604.1367.v1

density to enhance absorption, yet low enough to avoid photooxidation during prolonged outdoor exposure.

2.1.3. Vibrational Relaxation

In carbon-based photothermal materials, absorbed photon energy is dissipated as heat via vibrational relaxation, wherein lattice vibrations (phonon emission) serve as the primary energy dissipation channel (**Figure 2d**). This mechanism prevails in materials with strong electron–phonon coupling and low radiative recombination rates, and the broadband solar absorption and stable heat-generation characteristics of carbon-based systems render them well adapted to fluctuating outdoor solar irradiation [29]. Carbon-based materials used in anti-icing applications range from disordered carbons like candle soot and carbon black to graphitic forms such as CNTs, graphene, and graphite [27,30,59–77].

Candle soot, with its fractal-like hierarchical structure, traps sunlight through multiple internal reflections, yielding a temperature increase of 53 ℃ under 1 sun and ice-free operation at -50 ℃ [27]. Extending carbon-based photothermal functionality to lubricant-infused systems, a slippery photothermal surface fabricated by infusing silicone oil into a CNT/PDMS microporous array reaches over 160 ℃ under 1 W near-infrared irradiation while maintaining stable slippery performance [69]. Transparent applications pose a particular challenge. Strong visible absorption, essential for carbon-based photothermal performance, inherently conflicts with the high transmittance required for windows and optical devices.

2.1.4. Synergistic Photothermal Effects

While the three mechanisms discussed above offer distinct advantages, they also exhibit inherent limitations when employed in isolation. LSPR-based systems are typically constrained to specific wavelength ranges, semiconductor defect engineering often involves a trade-off with chemical stability, and carbon-based materials face challenges in achieving visible transparency. Many advanced photothermal systems integrate multiple energy dissipation pathways within a single material platform, thereby achieving broader spectral absorption and enhanced conversion efficiency (**Figure 2e**).

Multi-mechanism synergy is illustrated by the graphene@NiO/Ni surface, which combines photothermal, electrothermal, and magnetothermal conversion in a single hierarchical architecture. The graphene@NiO layer achieves over 90% solar absorption and reaches 64.7 ℃ under 1-sun illumination, while the inner Ni layer enables magnetothermal heating to 121.3 ℃ within 2 min [33]. Compositional engineering of MXenes offers an alternative route to enhanced performance: a double-transition-metal MXene exhibits elevated joint densities of states near the Fermi level, thereby achieving a surface temperature of 44 ℃ under 1 sun. Cu-MOF surfaces add another dimension: a narrow band gap (0.88 eV), π–π conjugation, and hierarchical light trapping together deliver over 98% solar absorption and a 65.5 ℃ temperature rise under 1-sun [78]. Precise control over each energy dissipation pathway is essential. Long-term operational stability will be equally critical for translating these synergistic designs into practical applications.

2.2. Performance Enhancement Strategies

Stable interfacial lubrication in practical anti-icing demands the collaborative optimization of multiple properties, most notably optical absorption and photothermal conversion efficiency [29]. Moreover, through rational system design, the heat generated by photothermal materials should be fully utilized for anti-icing and deicing [82]. To address the inherent performance trade-offs in practical scenarios, this section proposes four core design strategies that prioritize maintaining stable interfacial lubrication (**Figure 3**).

 doi:10.20944/preprints202604.1367.v1

2.2.1. Morphology Control of Nanomaterials

The optical absorption and photothermal efficiency of nanomaterials are intrinsically governed by their morphology. Rational morphology control enables LSPR spectral tuning, enhanced light trapping via multiple internal reflections, and optimization of the effective dielectric response. Morphological engineering strategies broadly fall into two categories: (1) precise shaping of individual nanostructures; (2) controlled assembly into ordered three-dimensional architectures.

The longitudinal LSPR mode of high-aspect-ratio nanoparticles is tuned across the visible-NIR range by varying the aspect ratio, thereby enabling spectral matching to solar irradiance for efficient light absorption (**Figure 3a1**) [83]. Alternatively, galvanic replacement of Ag templates with $HAuCl_4$ produces Au-Ag nanocages with LSPR peaks spanning 600-1200 nm and hollow interiors suitable for photothermal conversion (**Figure 3a2**) [84]. Beyond individual particle engineering, template-assisted deposition of gold onto nanoporous alumina creates a graded, close-packed distribution of nanoparticles. This yields an average absorbance of ~99% from 400 nm to 10 μm through densely hybridized LSPR modes and multiple internal reflections [85]. Future efforts should target high-throughput techniques that preserve key morphological features essential for broadband absorption and interfacial lubrication.

2.2.2. Doping and Defect Engineering

Doping and defect engineering tailor the electronic band structure of semiconductors to extend optical absorption into the visible-NIR region, thereby enhancing photothermal conversion (**Figure 3b**) [45]. The introduction of heteroatoms or lattice vacancies creates additional energy states within the band gap or modifies the band edges. This broadens the spectral response beyond the intrinsic absorption edge and promotes non-radiative relaxation, thereby enhancing heat generation [45].

 doi:10.20944/preprints202604.1367.v1

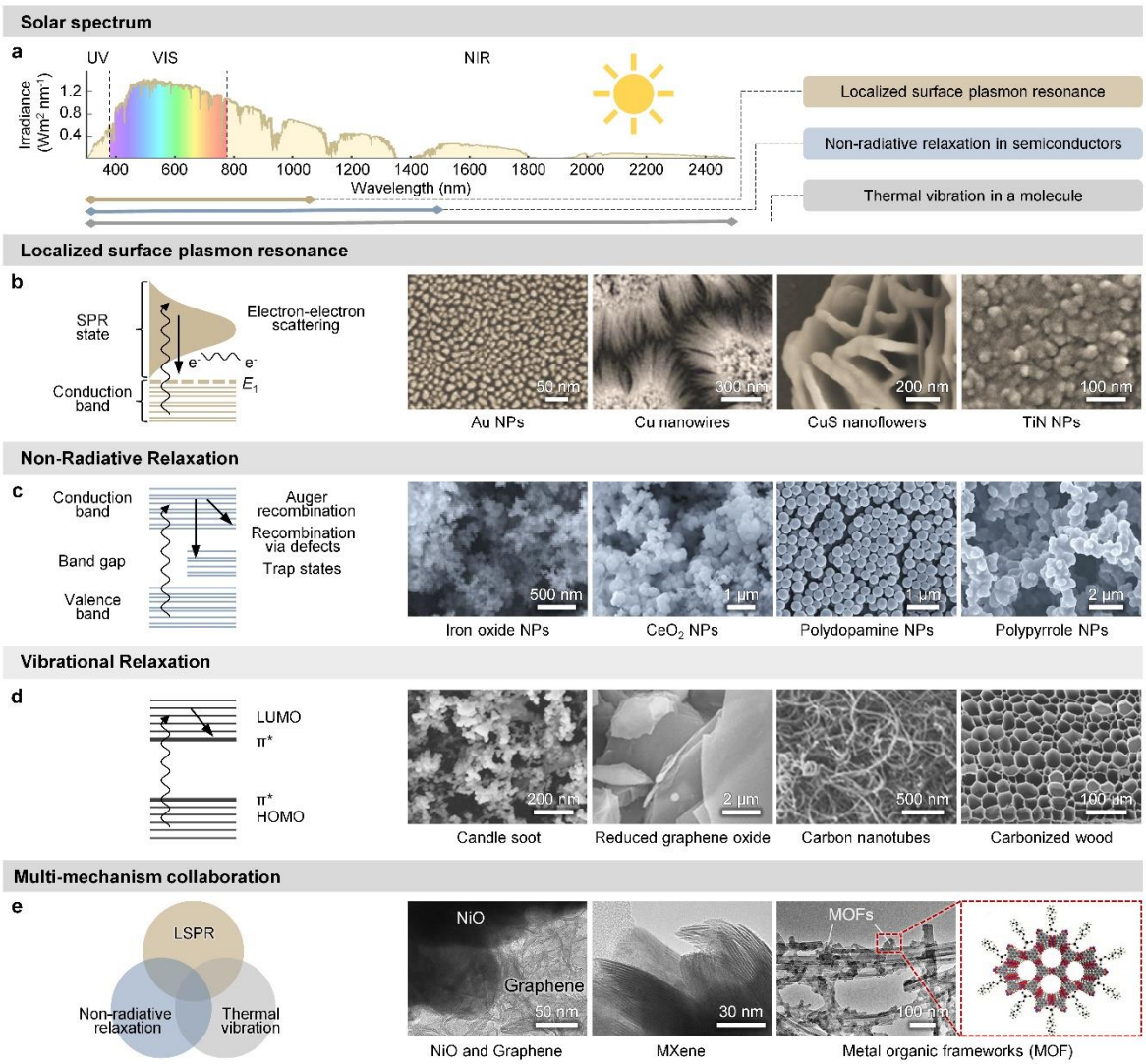

Figure 2. Classification and fundamental mechanisms of photothermal materials. (**a**) The AM 1.5 Global solar spectrum, highlighting the significant energy portion (49.9%) in the near-infrared (NIR) region. Reproduced with permission [31]. (**b**) Mechanism of plasmonic localized heating with representative material SEM images. Reproduced with permission [31,37,39,40]. (**c**) Non-radiative relaxation pathways in semiconductors with corresponding material morphologies. Reproduced with permission [28,51,54,79]. (**d**) Molecular vibrational relaxation (thermal vibration) mechanism exemplified by organic/polymeric materials. Reproduced with permission [27,68,76,80]. (**e**) Schematic and materials demonstrating synergistic photothermal effects combining multiple mechanisms. Reproduced with permission [33,78,81].

High-pressure hydrogenation of anatase TiO_2 introduces isolated Ti^{3+} defect centers that remain stable at room temperature, thereby enabling efficient photothermal conversion without noble-metal cocatalysts [86]. Structural disorder offers an alternative route to band-structure modulation, and ordered mesoporous black TiO_2 prepared via atmospheric H_2 annealing develops a disordered surface layer that narrows the band gap from 3.15 eV to 2.82 eV, substantially boosting visible-light absorption [87]. The key challenge remains the establishment of predictive relationships between defect configurations and photothermal efficiency to guide rational material design.

2.2.3. Hierarchical Micro/Nanostructure Engineering

Hierarchical micro/nanostructure engineering synergistically optimizes light capture, photothermal conversion, and surface wettability through the rational integration of multi-scale

 doi:10.20944/preprints202604.1367.v1

morphological features [88]. Microscale roughness, combined with nanoscale textures, forms structural light traps that promote multiple internal reflections and extend the optical path length, thereby enhancing broadband solar absorption. These architectures also entrap air pockets within the hierarchical textures, stabilizing the Cassie-Baxter state to impart superhydrophobicity and facilitate spontaneous meltwater removal.

Superblack wood, fabricated via delignification and carbonization at 1500 °C, transforms cell walls into vertically aligned carbon microfiber arrays with subwavelength dimensions, achieving a hemispherical reflectance of only 0.36% across the visible-NIR spectrum (**Figure 3c**) [80]. Building on this principle, superhydrophobic selective solar absorbers (SHSSA) integrate micro-cactus arrays, nano-spike textures, and plasmonic TiN nanoparticles to realize high solar absorptance (~90%), low infrared emittance (42%), and a temperature rise of 61 °C under 1-sun, enabling icephobicity down to -60 °C [41]. Robust composite coatings take this further. In CNT/TiN@polydimethylsiloxane (PDMS) porous networks, plasmonic coupling between TiN and CNTs lowers visible reflectance to 0.66% and drives heating to 70.1 °C under 1-sun. The improved filler–matrix interface also imparts mechanical durability [89]. The long-term stability of hierarchical structures under repeated icing/deicing cycles remains a key challenge.

2.2.4. System Integration Design

System integration design rationally matches material components with structural characteristics to achieve multifunctional performance within a single platform. Rather than optimizing individual properties in isolation, this approach synergistically couples broadband light absorption with interfacial thermal management, superhydrophobicity, and mechanical durability. The key lies in engineering a layered or hierarchical architecture where each component fulfills a distinct role while collectively enabling efficient photothermal conversion and stable interfacial lubrication (**Figure 3d**).

A photothermal trap laminate exemplifies this integrated design philosophy (**Figure 3d1**). Comprising a cermet selective absorber ($\alpha = 95\%$, $\varepsilon \approx 3\%$), an aluminum thermal spreader, and a foam insulation backing, the trap confines solar heat at the ice–substrate interface while suppressing transverse thermal losses. The thin absorber and spreader ensure rapid thermal response and lateral heat conduction, generating a lubricating melt layer within seconds under 1-sun illumination [26]. A complementary integration strategy employs solution-processed all-ceramic plasmonic metamaterials (**Figure 3d2**). An ultrathin TiN nanoparticle film (~120 nm) is assembled on a TiN reflector and capped with a SiO_2 anti-reflection coating. The synergy of in-plane plasmon coupling and out-of-plane Fabry-Pérot resonances yields a solar absorptance of 95% and an infrared emittance of only 3% at 100 °C, enabling a steady-state temperature of 91 °C under 1-sun and stable operation up to 727 °C [40]. Extending such integrated designs to curved substrates and ensuring long-term stability under cyclic stresses remains a key challenge.

 doi:10.20944/preprints202604.1367.v1

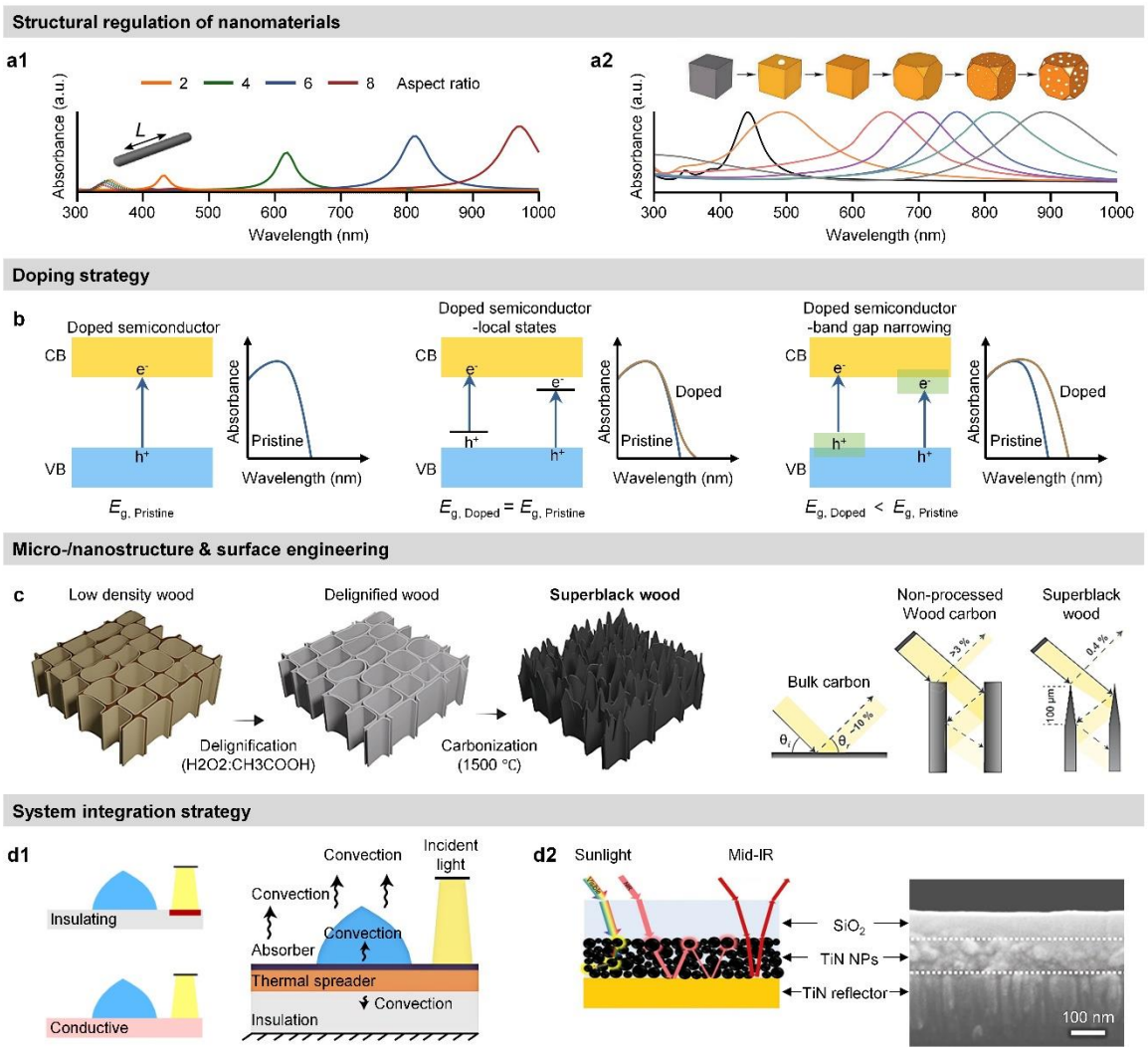

Figure 3. Strategies for enhancing photothermal performance. (**a1**) Tuning of localized surface plasmon resonance (LSPR) spectra via control of nanorod aspect ratio. Reproduced with permission [83]. (**a2**) UV-vis absorbance modulation of noble metal nanostructures through compositional engineering. Reproduced with permission [84]. (**b**) Band structure engineering (doping, defect creation) to broaden optical absorption in semiconductors. Reproduced with permission [29]. (**c**) Superblack wood for efficient light trapping and minimization of reflection. Reproduced with permission [80]. (**d1**) Schematic of the photothermal trap on the base substrate, showing its laminate structure and heat transfer mechanisms. Reproduced with permission [26]. (**d2**) Schematic of the SSA and cross-sectional SEM image of the prepared SSA. Reproduced with permission [40].

3. Anti-Icing and Deicing Mechanisms

The anti-icing/deicing process of photothermal superwetting surfaces comprises three consecutive stages: droplet dynamics control (pre-icing), ice nucleation suppression with thermal management (during icing), and low-adhesion ice detachment (post-icing) [35]. The “water as a lubricating layer” strategy is central to the deicing stage. Localized photothermal heating generates a continuous meltwater film at the ice-substrate interface, converting high-adhesion solid-solid contact into low-friction solid-liquid-solid contact [29]. This mechanism drastically reduces ice adhesion strength, enabling efficient deicing with minimal energy consumption. **Figure 4** summarizes the stagewise mechanisms, working principles, and performance verification. This chapter provides a systematic analysis of these anti-icing and deicing mechanisms.

 doi:10.20944/preprints202604.1367.v1

3.1. Droplet Dynamics Control

Dynamic regulation of supercooled droplets is the primary anti-icing barrier. It minimizes droplet retention prior to ice nucleation, thereby inhibiting icing at its source [15,28,90]. Even if icing occurs, this mechanism creates stable interfacial conditions that facilitate the formation of a uniform lubricating water film during subsequent photothermal deicing.

3.1.1. Supercooled Droplet Rebound

Supercooled droplet rebound is the key active anti-icing mechanism in the pre-ice nucleation stage. It minimizes the liquid-solid contact time (τ_c), enabling droplet detachment before heterogeneous ice nucleation at the interface [15,17]. This process is governed by the time-scale competition between droplet retraction and ice nucleation (**Figure 4a1**). Stable rebound requires a robust Cassie non-wetting state, ultra-low adhesion, and structural integrity.

Basic studies have confirmed that SHS with ordered micro-nano structures can maintain an ice-free state at -25 to -30℃ via droplet rebound [15]. Relevant studies have revealed the fragility of droplet pinning and the wetting transition under extreme supercooling [12]. These issues can be alleviated through microstructure design. Latest advances further break through the limits of extreme-environment adaptability. Biomimetic microstructures achieve continuous droplet repellency with ultra-low interfacial adhesion [90]. The current core challenge is maintaining structural stability under repeated droplet impacts, especially in low-temperature, high-humidity environments.

3.1.2. Coalescence-Induced Droplet Jumping

Coalescence-induced droplet jumping is a passive, energy-free pre-icing mechanism. It harnesses the surface energy released during the coalescence of adjacent condensed microdroplets on SHS, propelling the merged droplet away from the substrate [13]. As shown in **Figure 4a2**, this spontaneous removal reduces the residence time and surface coverage of condensed water, thereby delaying ice nucleation and frost propagation, while preserving the superhydrophobic interface for subsequent formation of a lubricating water film. Stable jumping requires a robust Cassie-Baxter state with minimal contact-line pinning, enabling merged droplets to overcome adhesion and gain sufficient upward kinetic energy [91].

Foundational studies have verified that condensed droplets on SHS can achieve jumping velocities up to 1 $m \cdot s^{-1}$ [13]. This established the inertial-capillary scaling of jumping velocity and the core mechanism of surface-energy-to-kinetic-energy conversion. Subsequent research translated this mechanism into scalable engineered surfaces with ~30% enhanced condensation heat transfer. However, a critical limitation was identified: high supersaturation ($S > 1.12$) leads to surface flooding and a Wenzel-state transition, which completely suppresses jumping behavior [91]. To address this instability, hierarchical photothermal SHS integrating coalescence-induced jumping and efficient photothermal absorption has been developed. These maintain a dry-area fraction above 80% during condensation [28]. As shown in **Figure 4a3**, they achieve ice-free performance even at -50℃ and high humidity. The key unresolved challenge is maintaining stable jumping performance under high-humidity and low-temperature conditions.

 doi:10.20944/preprints202604.1367.v1

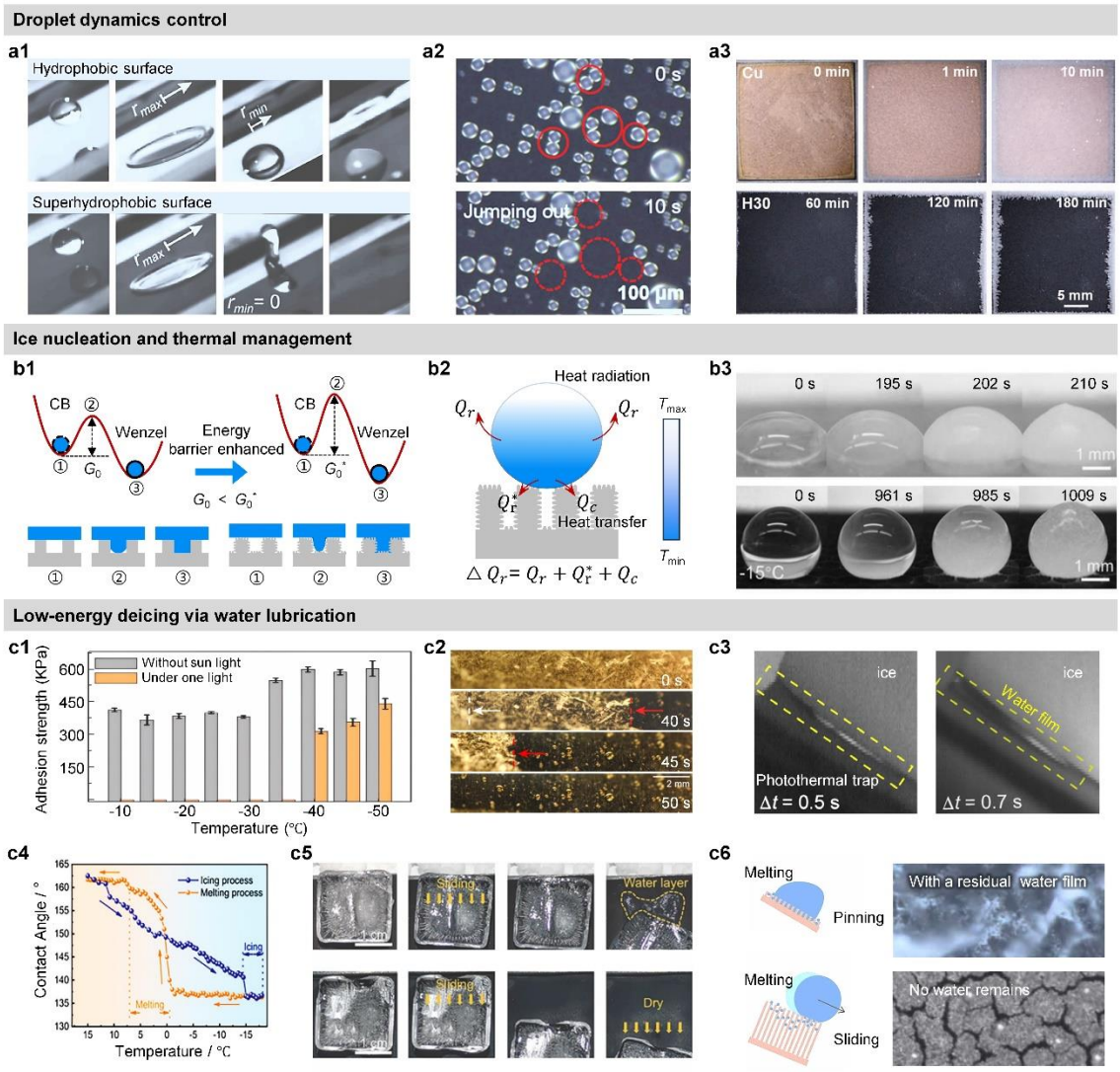

Figure 4. Anti-icing/deicing mechanisms of photothermal superwetting surfaces. (**a1**) Supercooled droplet impacting a cold tilted surface: freezes on a hydrophobic surface but rebounds on SHS. Reproduced with permission [15]. (**a2**) Removal of condensed droplets via coalescence-induced jumping. Reproduced with permission [28]. (**a3**) Long-term anti-frosting performance on Cu and H30 surfaces. Reproduced with permission [28]. (**b1**) Dual-energy-barrier design: open microcones connect air pockets to the atmosphere, whereas closed micropores trap air pockets within three-phase interfaces. Reproduced with permission [92]. (**b2**) Heat transfer pathways on SHS: solid-liquid conduction (Q_c), droplet-air radiation (Q_r), and convection (Q_c). (**b3**) Icing delay on surfaces before and after abrasion cycles. Reproduced with permission [4]. (**c1**) Ice adhesion strength on a photothermal coating with/without sunlight. Reproduced with permission [56]. (**c2**) Melting of a frost layer on the photothermal trap. Reproduced with permission [26]. (**c3**) The liquid layer at 0.5 to 0.7 s after the start of melting on the photothermal trap. Reproduced with permission [26]. (**c4**) Wettability transitions on E/O@TiN during icing (blue) and melting (orange). Reproduced with permission [43]. (**c5**) Solar deicing on a tilted surface under 1-sun. Reproduced with permission [43]. (**c6**) Under sunlight, droplets roll on nanowires (no residue) but pin on other nanostructures (water film remains after deicing). Reproduced with permission [37].

3.2. Ice Nucleation and Thermal Management

Ice nucleation inhibition and interfacial thermal management form the second anti-icing barrier. Through surface-structure design and material optimization, this stage raises the thermodynamic energy barrier for heterogeneous ice nucleation and regulates the interfacial temperature distribution [55,92,93]. These measures delay ice crystal formation and propagation, while providing a

 doi:10.20944/preprints202604.1367.v1

thermodynamic basis for the rapid, uniform formation of a lubricating water film during subsequent photothermal deicing.

3.2.1. Ice Nucleation Suppression

Suppressing or delaying heterogeneous ice nucleation is key to passive anti-icing. It minimizes active nucleation sites and maximizes the free-energy barrier through surface chemistry and topography. At the same time, it maintains the integrity of the superhydrophobic interface, thereby supporting the stable formation of the lubricating water film during subsequent photothermal deicing [92–94].

Early approaches leveraged the Cassie-Baxter state to reduce solid-liquid contact area, achieving significant icing delays via trapped air pockets (**Figure 4b1**) [16]. Further dual-energy-barrier designs achieve icing delays over 27,000 s at -15℃ through sequential liquid pinning that decouples wetting transition and stabilizes the Cassie state [92]. However, this passive strategy is vulnerable to high humidity and prolonged cooling, as condensate infiltration or a Wenzel-state transition leads to rapid ice formation [93].

To address this, research has shifted to actively elevating the nucleation energy barrier. Nanoscale interfacial engineering with feature sizes matching the critical ice nucleus significantly increases the free-energy barrier, enabling supercooled water to remain unfrozen for ≥1 h at -25℃ without energy input. This confirms that interfacial size, not just wettability, is key to controlling ice nucleation [94]. The key remaining challenge is the low-cost, large-area fabrication of dual-energy-barrier surfaces.

3.2.2. Heat Transfer and Temperature Distribution

Interfacial heat transfer and temperature distribution directly regulate ice nucleation and ice crystal growth. They also determine the formation efficiency of the interfacial lubricating water film under photothermal irradiation, serving as the key link between passive anti-icing and active photothermal deicing [4,16,55,78,93,95]. As illustrated in **Figure 4b2**, hierarchical micro-nano structures play a dual role in thermal management by reducing heat transfer to delay ice nucleation while enhancing localized heating to facilitate meltwater film formation.

Early studies exploited the passive thermal-barrier effect of superhydrophobic structures to delay freezing, but these structures are vulnerable to wetting failure in long-term cold, humid environments [16]. The integration of photothermal materials introduces active thermal regulation: interfacial heating inhibits ice nucleation and prolongs droplet liquid-phase duration (**Figure 4b3**). For example, photothermal trap coatings suppress ice nucleation even at -40℃ under sunlight [30]. Recent work has also revealed a self-recovery mechanism for the thermal barrier during cycling, further improving cyclic performance [93]. Accurately characterizing the coupled relationship between photothermal conversion and heat loss remains a key challenge.

3.3. Low-Energy Deicing via Water Lubrication

The “water as a lubricating layer” strategy achieves low-energy deicing via a sustainable in situ meltwater film, avoiding the wetting failure of SHS and the lubricant depletion of SLIPS [12]. Localized photothermal heating melts the ice-substrate interface, forming a water film that reduces ice adhesion to <10 kPa (**Figure 4c1**) and enables passive detachment by gravity or wind [56]. From a tribological perspective, full-film fluid lubrication requires a continuous water film exceeding the surface roughness; otherwise, boundary lubrication leads to high adhesion.

3.3.1. Defrosting and De-Snowing

Unlike bulk ice, frost and snow have loose, porous structures [5,32,96], which result in only shallow interlocking with surface micro-nano structures and thus weak adhesion [37]. Under sunlight, the surface of photothermal materials can heat up rapidly, promoting the rapid melting of

 doi:10.20944/preprints202604.1367.v1

frost layers/snow. The melted water rapidly shrinks and curls at the hydrophobic interface (**Figure 4c2**). Taking advantage of the surface's low adhesion, it spontaneously strips away, achieving residue-free and highly efficient defrosting/de-snowing [37].

Nevertheless, the loose porous structure of frost and snow causes multiple scattering of incident sunlight. This reduces the effective light flux reaching the underlying photothermal coating. The defrosting duration is directly correlated with the initial frost thickness, with thinner frost layers corresponding to significantly shorter defrosting times [32]. The effects of frost/snow thickness on sunlight reflection, light absorption, and photothermal conversion efficiency remain unclear and warrant systematic investigation.

3.3.2. Shell-Like Ice Detachment

Unlike frost or snow, shell-like ice formed by freezing rain or condensed water films exhibits a dense, non-porous microstructure that establishes conformal solid-solid contact with the substrate, resulting in high interfacial adhesion strength [26,43]. Photothermal surfaces address this challenge through a fundamentally different pathway. Rather than melting the entire ice volume, they preferentially generate an ultrathin lubricating water film at the ice-substrate interface upon solar illumination (**Figure 4c3**). This interfacial melt layer dramatically reduces ice adhesion and enables the still-frozen ice shell to slide off under gravity, wind, or mild vibration, thereby minimizing the energy required for complete ice removal [26,90].

A photothermal trap laminate comprising a selective absorber, a thermal spreader, and an insulating backing was developed to confine solar heat at the interface, thereby initiating ice sliding within seconds of illumination [26]. The stable Cassie state maintained during the melting process is essential for preventing meltwater penetration and residual pinning. On triple-scale etched/oxidized TiN-coated (E/O@TiN) surfaces, downward-captured bubbles from melting ice rebuild interfacial air pockets, driving spontaneous dewetting back to the non-wetted Cassie state (**Figure 4c4**). Owing to this property, millimeter-thick ice blocks detach cleanly from a 15° tilted E/O@TiN surface within 500 s under 1-sun (**Figure 4c5**) [43].

Nevertheless, thick ice layers attenuate incident sunlight and delay interfacial melting, while high forced convection narrows the operational temperature range [26]. Additionally, cyclic refreezing of meltwater risks gradual degradation of Cassie-state stability [43].

3.3.3. Self-Driven Meltwater Management

Residual meltwater refreezes at sub-zero temperatures, damaging the SHS and preventing the formation of a lubricating water film in subsequent cycles. Self-driven meltwater removal leverages surface superhydrophobicity and interfacial forces to achieve spontaneous detachment without external intervention, ensuring reversible recovery of the initial interfacial state and cyclic sustainability [37].

The core mechanism is the spontaneous recovery of the Cassie-Baxter state during the ice-water phase transition. Meltwater remains non-wetting and easily rolls off under minimal driving forces [93]. Hierarchical copper nanowire assemblies combine efficient photothermal conversion, high lateral thermal conductivity, and superhydrophobicity. They enable complete spontaneous shedding of melted frost with nearly 100% defrosting efficiency and zero residue (**Figure 4c6**) [37].

Thermoresponsive paraffin-based phase-change coatings undergo solid–liquid transition under photothermal or electrothermal stimulation. This transition breaks the mechanical interlocking between meltwater and surface micro-nanostructures. It also achieves thorough surface drying and reversible recovery of the Cassie-Baxter state [54]. Key challenges include validating performance under real-world conditions and ensuring long-term durability over hundreds of icing/melting cycles.

 doi:10.20944/preprints202604.1367.v1

4. Key Challenges and Development Strategies

Despite laboratory progress, photothermal superwetting anti-icing surfaces based on the "water as a lubricating layer" strategy face three industrial bottlenecks: mechanical durability, all-weather applicability, and optical transparency [29,35,97]. These directly hinder the stable formation of the interfacial lubricating water film. The main obstacles include structural degradation under mechanical stress, insufficient deicing capability in low- or no-light conditions, and the inherent trade-off between solar absorption and visible transparency. This chapter discusses these challenges and the corresponding material/structural design strategies, with a focus on how they regulate water film stability and lubrication performance.

4.1. Mechanical Durability

Mechanical durability is the primary bottleneck for practical applications. The micro-nano rough structures of photothermal superwetting surfaces are inherently brittle, leading to rapid performance degradation under abrasion, impact, or shear stress [82,98]. Such damage impairs the superhydrophobic interface required to form a lubricating water film, resulting in water-film impregnation, lubrication failure, and increased ice adhesion. Recent research has focused on two complementary strategies to improve long-term durability: wear resistance enhancement and self-healing functionalization (**Figure 5**).

4.1.1. Wear-Resistant Design

Current wear-resistant design strategies for durable icephobic coatings fall into three categories: (1) high-strength matrix design [49,52,79,99–101]; (2) hierarchical self-similar structure [32,62]; and (3) protective microstructure armor strategy [4,44,102].

High-strength matrix design achieves uniform stress distribution and protects micro-nano structures through high-toughness, high-adhesion polymer matrices (**Figure 5a**). Several approaches fall under this category. High-adhesion resins, for instance, can anchor functional coatings, for example, a sandpaper-inspired epoxy matrix in which semi-embedded SiC microparticles shield a spray-coated TiN nanoparticle layer [99]. Composite encapsulation operates differently: cross-linked PDMS fills cracks in CeO_2 coatings, thereby maintaining structural integrity [79]. For flexible substrates, mussel-inspired polydopamine anchoring layers offer an effective solution [101]. Core challenges include optimizing filler–matrix interfacial compatibility to prevent delamination under cyclic loading, and mitigating degradation caused by UV irradiation and thermal cycling.

Hierarchical self-similar structure strategy avoids overreliance on matrix strength [103]. A self-similar reservoir design enables in situ regeneration of superhydrophobic and photothermal properties after surface wear, extending coating service life. As shown in **Figure 5b**, a representative example is the bioinspired THMC film [62], which has a hierarchical self-similar structure. It retains a water contact angle of 148.7° and a photothermal temperature of 79.9℃ after 300 cm of linear abrasion, demonstrating effective in situ regeneration of hydrophobicity and stable photothermal performance. The core challenge is maintaining functional uniformity through the coating thickness.

 doi:10.20944/preprints202604.1367.v1

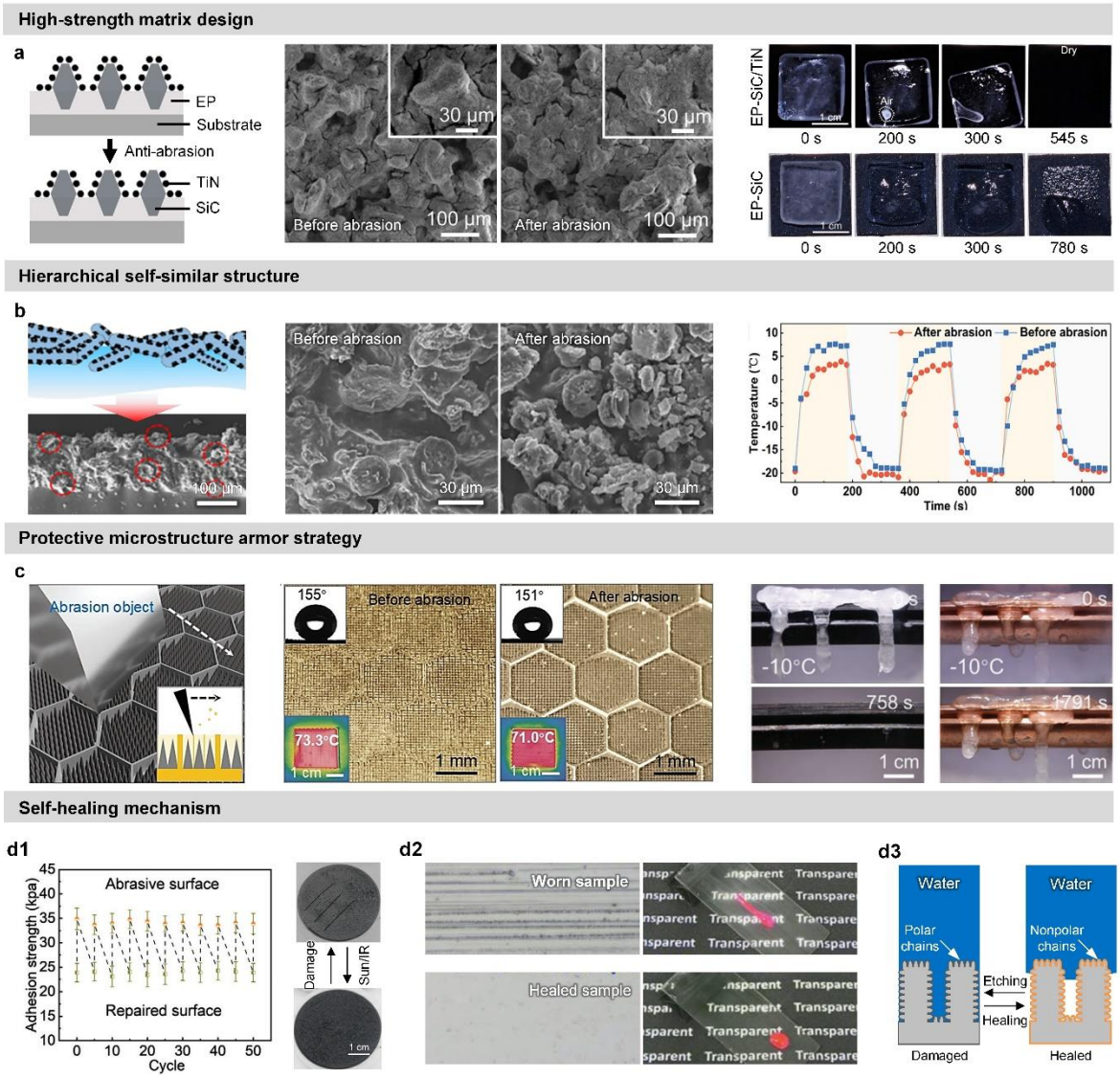

Figure 5. Material and structural strategies for enhancing durability. (**a**) Sandpaper-inspired armor structure (SiC/TiN) with SEM showing wear resistance, enabling durable solar-driven deicing. Reproduced with permission [99]. (**b**) THMC design with wear-resistant structure and retained photothermal heating after abrasion. Reproduced with permission [62]. (**c**) Photothermal SHS with honeycomb macrostructure and micro-spines for mechanical robustness and deicing on transmission lines. Reproduced with permission [4]. (**d1**) Adhesion strength variation during 50 alternating abrasion/repair cycles on the CCP surface. Reproduced with permission [68]. (**d2**) MXene-SOPS-coated glass surface before (worn) and after healing. Reproduced with permission [107]. (**d3**) Plasma etching and healing process schematic. Reproduced with permission [51].

A protective microstructure armor strategy decouples mechanical robustness from interfacial nonwettability via rigid microscale frameworks, thereby protecting fragile functional nanostructures and preserving superhydrophobic and photothermal properties under shear stress. As shown in **Figure 5c**, a honeycomb-protected microspine array (MAHC) was designed to enhance mechanical durability [4]. The rigid honeycomb framework reduces the maximum stress on the microspines by approximately 66.7%, enabling the surface to maintain superhydrophobicity and photothermal deicing after 200 linear abrasion cycles. The core challenge lies in the high cost of large-scale manufacturing and limited adaptability to complex curved-surface components.

 doi:10.20944/preprints202604.1367.v1

4.1.2. Self-Healing Surfaces

Self-healing photothermal coatings restore damaged surface structure, wettability, and photothermal performance, overcoming a key bottleneck for outdoor applications. Current strategies fall into two categories: (1) extrinsic healing, which relies on pre-embedded reparative agents [50,104–106]; and (2) intrinsic healing, which uses dynamic characteristics of the coating matrix (photothermally activated polymer chain reconfiguration or reversible bond dynamics), where the photothermal effect accelerates healing even at sub-zero temperatures [51,70,75,107,108].

For extrinsic healing, a reservoir of reparative agents is built into the coating. A typical system uses a porous cellulose acetate substrate with a carbon nanotube (CNT) photothermal layer and paraffin wax as the agent (**Figure 5d1**). Under 1-sun, the CNT layer melts the paraffin, which flows into scratches and resolidifies, completing healing within 16 s. This system works even at -22℃ under near-infrared irradiation and maintains its performance after 50 abrasion-repair cycles [68].

Intrinsic healing is further divided into two types. The first relies on photothermal activation of polymer chain reconfiguration in the absence of external agents. For example, a transparent coating with ultrathin MXene multilayers and an omniphobic slippery layer (**Figure 5d2**) heats to 76.5 ℃ under 1.5 sun, inducing chain migration that repairs scratches within 2 h and restores slippery properties at -30 ℃ [107]. The second type uses dynamic reversible bonds in the polymer matrix. A coating based on a PDMS-IPDI-TFB supramolecular network (hydrogen and imine bonds) and PDA nanoparticles (**Figure 5d3**) recovers superhydrophobicity within 15 min under 1-sun after plasma etching[51].

The key challenge is achieving fast, stable healing at ultra-low temperatures (below -30 ℃) with long-term durability, while balancing mechanical robustness with the chain mobility or bond dynamics required for healing.

4.2. All-Weather Applicability

The inherent intermittency of solar irradiation is the key limitation of purely photothermal deicing systems [45,109,110]. Under insufficient illumination conditions (nighttime, overcast days, or extremely low temperatures), a stable lubricating water film cannot form, resulting in the failure of interfacial lubrication and loss of deicing capability. Representative designs for all-weather anti-icing/deicing are summarized in **Figure 6**.

4.2.1. Photo-Electrothermal Coupling

As shown in **Figures 6a1** and **6a2**, photo-electrothermal coupling combines solar-driven photothermal conversion with electrical Joule heating for all-weather anti-icing/deicing. This dual-heat-source system ensures stable interfacial heating and continuous formation of a lubricating water film under fluctuating illumination, while maximizing solar energy utilization and minimizing energy consumption [6].

Conductive materials for electrothermal heating can be divided into carbon-based [55–61] and metal-based [2,111–113] systems (**Figures 6b1** and **6b2**). For carbon-based materials, laser-induced graphene (LIG) films exhibit controllable and stable temperature rise with increasing power density, reaching 43.2 ℃ at a low applied power density of 0.135 W/cm^2 (**Figure 6c1**) [74]. Similarly, a fluorine-free bilayer coating achieves rapid and uniform Joule heating at subzero temperatures, further validating the high deicing efficiency of carbon-based designs (**Figure 6c2**) [42]. For metal-based systems, silver nanowire (Ag NW) networks offer faster temperature rise and higher heating efficiency. For instance, an armored surface structure protecting the Ag NW conductive layer enables rapid deicing (132.3 ℃ at 0.25 W/cm^2 within 14 s at -20 ℃) [2]. Metal nanowire networks are particularly advantageous for fabricating transparent photoelectric-thermal deicing materials due to their high conductivity, efficient Joule heating, and optical transmittance [109]. **Figure 6d** further demonstrates the all-weather deicing performance enabled by this photo-electrothermal synergy.

 doi:10.20944/preprints202604.1367.v1

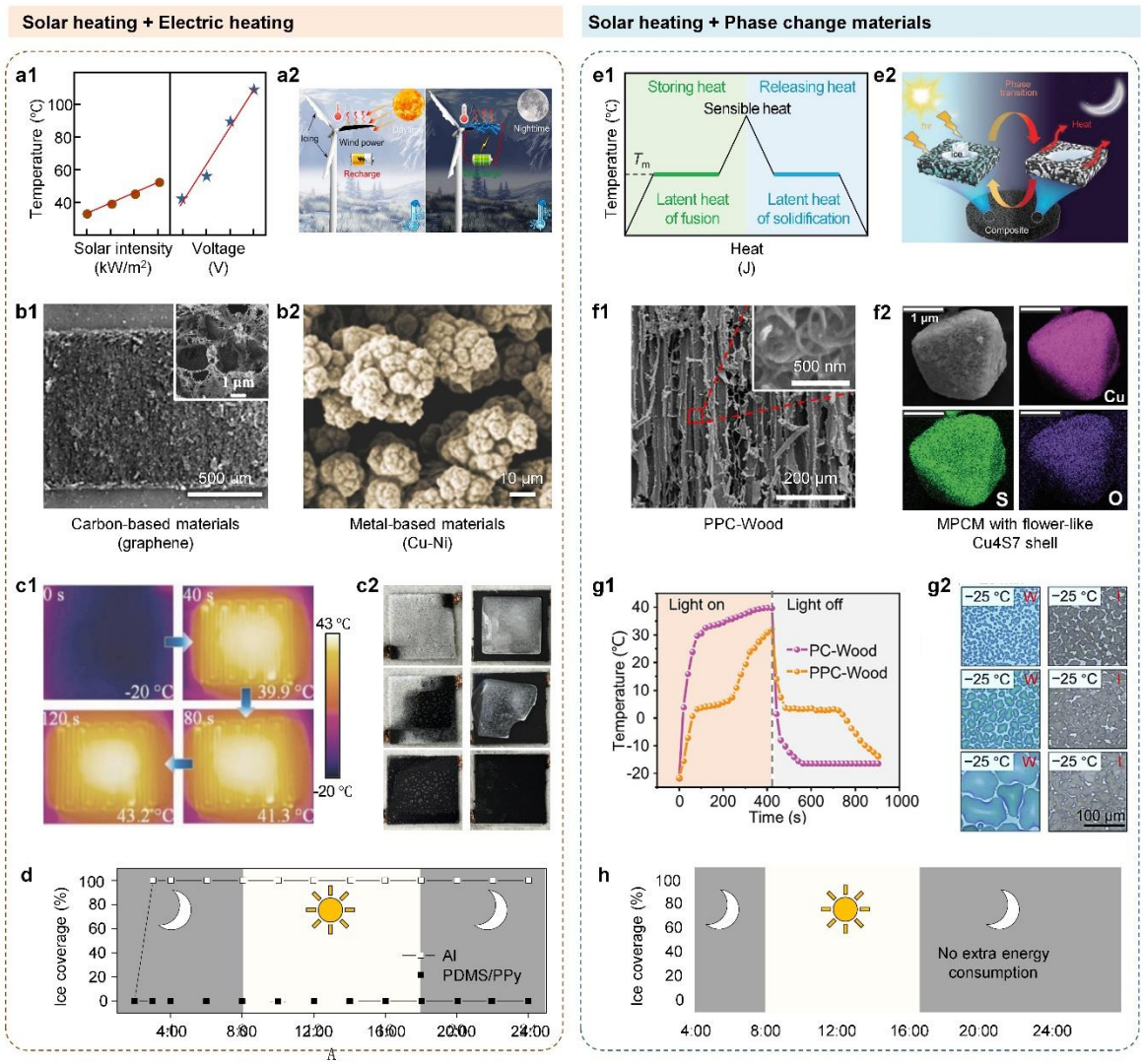

Figure 6. Design paradigms for all-weather applicability. (**a1**) Photothermal and electrothermal response. Reproduced with permission [6]. (**a2**) Schematic of photothermal/electrothermal superhydrophobic coating. Reproduced with permission [6]. (**b1**) Laser-ablated graphene network. Reproduced with permission [74]. (**b2**) Cu-Ni@PET. Reproduced with permission [112]. (**c1**) Capacitance change during ice growth. Reproduced with permission [74]. (**c2**) Electrothermal defrosting and deicing. Reproduced with permission [42]. (**d**) All-weather deicing performance. Reproduced with permission [29]. (**e1**) Latent heat storage and release of PCMs. Reproduced with permission [35]. (**e2**) Solar-thermal energy conversion and storage in PCM. Reproduced with permission [30]. (**f1**) CNT-coated PP-Wood. Reproduced with permission [114]. (**f2**) Microencapsulated PCMs with Cu_4S_7 shell. Reproduced with permission [39]. (**g1**) Temperature variation at -25℃ under light on/off. Reproduced with permission [114]. (**g2**) Condensation and frost formation with light cycling. Reproduced with permission [94]. (**h**) All-weather deicing performance. Reproduced with permission [71].

Key challenges include improving heating uniformity under extreme conditions, reducing energy consumption at ultra-low temperatures, and developing scalable fabrication methods for robust multilayer coatings without compromising mechanical flexibility.

4.2.2. Phase Change Materials

Phase change materials (PCMs) address solar intermittency through high latent heat storage. As shown in **Figures 6e1** and **6e2**, PCMs store excess photothermal energy during illumination and release it at night or during low-temperature periods, thereby extending the anti-icing window to non-illuminated times while maintaining the interface temperature above the melting point to support the stable formation of a lubricating water film [30,35].

 doi:10.20944/preprints202604.1367.v1

As shown in **Figures 6f1** and **6f2**, to prevent liquid leakage during phase transitions, PCMs are typically confined within porous scaffolds [30,54,68,114] or sealed inside micro- or nanocapsules [38,39,53,71,115]. For example, a biomimetic layered coating with a photothermal superhydrophobic top layer and a PCM bottom layer delays ice nucleation by releasing latent heat. A solar-driven expanded graphite/paraffin/PDMS composite achieves a freezing delay of over 2 hours at -40℃ after 1-sun irradiation [30], and photothermal storage microcapsules maintain anti-icing function even in complete darkness [38,39,53]. **Figure 6g1** shows the temperature variation of a PCM-loaded surface under light on/off cycles at -25℃, where a distinct plateau near the freezing point indicates latent heat release [114]. This latent heat release is responsible for the delayed ice nucleation observed in **Figure 6g2**, where condensation freezing is postponed even under light-off conditions [94]. **Figure 6h** further demonstrates all-weather deicing performance enabled by PCM integration [30].

Beyond thermal effects, the volume change during PCM phase transition generates local shear stress at the ice-coating interface, reducing ice adhesion strength and promoting low-force ice detachment [116]. Key challenges include optimizing the PCM microstructure to simultaneously maximize heat-transfer efficiency and interfacial ice-detachment shear stress.

4.3. Transparent Photothermal Materials

In applications such as photovoltaic panels, automotive windows, and optical sensors, an inherent trade-off exists: high solar absorptance is required to promote the formation of a lubricating water film, while simultaneously high visible-light transmittance is needed. This trade-off has driven the development of two primary classes of transparent photothermal materials [5,36,94,117]. **Figure 7a** presents both the ideal spectral design and the multilayer structure of a typical transparent photothermal SHS.

Transparent photothermal superhydrophobic composites combine near-infrared (NIR) selective absorption nanomaterials with a hydrophobic matrix. These nanomaterials include Au NPs [31], MXene [107,118], PPy NPs [56], titanium oxide layers [119], and cesium-doped tungsten trioxide (CWO) NPs [5] (**Figure 7b**). This combination reduces visible light scattering while maintaining superhydrophobicity and anti-icing performance. For example, the CWO/silver nanowire composite film achieves a visible light transmittance of over 70% and excellent UV-NIR absorption [111]. As shown in **Figure 7c**, the moiré-structured film has a visible-light transmittance of 93% and enables efficient photovoltaic anti-icing at -20℃ [5].

Liquid-infused transparent slippery interfacial materials offer another approach. The ultrathin MXene multilayer film integrated with an all-hydrophobic slippery coating exhibits a transmittance of over 77% at 550 nm. It also provides efficient photothermal conversion (about a 31℃ temperature rise under 1-sun irradiation) and photothermal self-healing [107]. A monolayer self-assembled MXene film (2.5 nm thick) achieves 82.5% visible transmittance and 25.1℃ photothermal rise under 1-sun; when combined with a slippery surface, it enables rapid ice shedding (85 s at -20℃) and anti-fogging [118].

 doi:10.20944/preprints202604.1367.v1

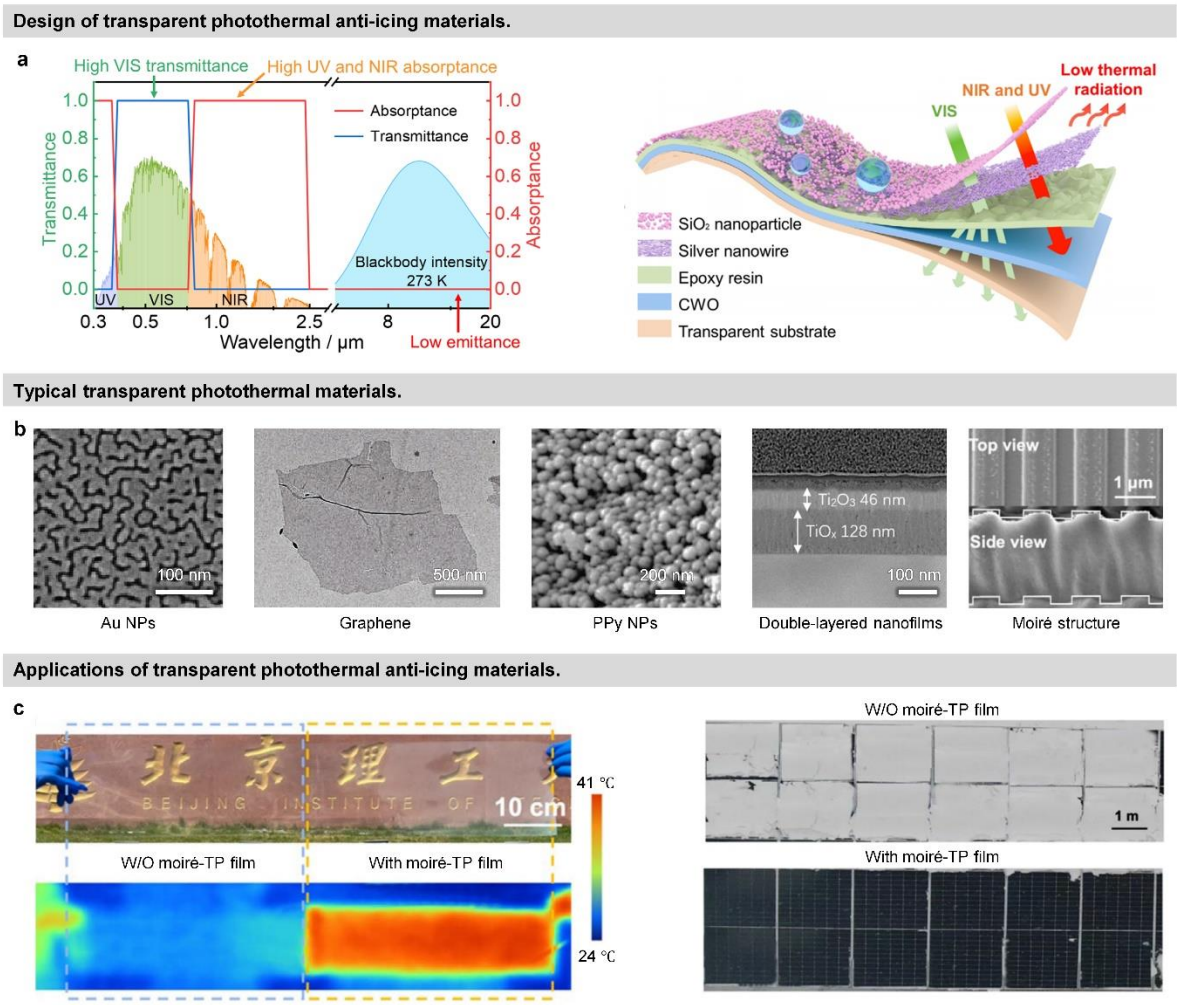

Figure 7. Toward highly transparent photothermal anti-icing surfaces. (**a**) Ideal spectra and multilayer structure of the transparent solar thermal metasurface. Reproduced with permission [36]. (**b**) SEM images of representative nanomaterials for transparent photothermal anti-icing materials. Reproduced with permission [5,31,56,107,119]. (**c**) Large-scale application and demonstration of a transparent photothermal film (moire-TP) for deicing solar panels in real-world conditions. Reproduced with permission [5].

The main challenges are twofold: balancing visible transparency with solar absorption and superhydrophobic durability, and ensuring enough photothermal input to sustain lubricating film formation. Additionally, low-cost and scalable fabrication methods for large-area, flexible substrates remain to be developed.

5. Future Directions

To achieve the industrial deployment of photothermal superwetting anti-icing surfaces based on the "water as a lubricating layer" strategy, critical breakthroughs in five core areas are required. All these breakthroughs focus on two core priorities: deepening the fundamental understanding of interfacial water lubrication mechanisms and advancing engineering applications of this technology [10]. The future development directions and potential engineering applications are projected in **Figure 8**.

5.1. Multi-Dimensional Design

The core goal of future material design is the stable formation and long-term maintenance of the interfacial lubricating water film. As shown in **Figure 8a1**, the core implementation path is the

 doi:10.20944/preprints202604.1367.v1

rational engineering of hierarchical micro/nanostructures to synergistically enhance photothermal conversion efficiency and mechanical wear resistance [89,110]. Such designs help resolve the trade-off between performance and structural complexity, adapt better to weak-light conditions, and lower full-cycle energy consumption [93,120].

As complementary and expandable strategies shown in **Figure 8a2**, future material design should further incorporate the following four dimensions: (1) machine-learning-assisted multi-objective optimization of hierarchical structures [121,122]; (2) synergistic regulation of multi-mode anti-icing/deicing mechanisms [10,123–125]; (3) in situ dynamic sensing of icing and interfacial states [126]; and (4) all-season, full-lifecycle service performance design [33,34]. Priority should be given to establishing a quantitative evaluation system for the wear resistance of photothermal micro- and nanostructures.

5.2. Fabrication for Practical Application

Practical deployment of photothermal, superhydrophobic, and anti-icing materials requires scalable, low-cost fabrication techniques applicable to complex substrates. Among various methods, roll-to-roll processing stands out as a particularly promising route for large-area fabrication due to its high throughput, continuous operation, and compatibility with flexible substrates (**Figure 8b1**) [5,132].

As shown in **Figure 8b2**, conformal materials are essential for non-planar substrates, including electrical insulators, aircraft wings, and turbine blades [1,32,127,128]. Flexible films can maintain superhydrophobicity even under large deformation [62,100]. Substrate-adaptive techniques, including spray coating, can work well on uneven surfaces [32,49]. Key challenges include long-term durability under environmental stress and the trade-off between conformality and performance.

5.3. In Situ Characterization

To fully understand the interfacial phenomena, characterization techniques must be capable of synchronously capturing molecular-scale ice nucleation (**Figure 8c1**), microscale droplet/ice dynamics, and the formation of the lubricating water film under real environmental conditions [96,129]. Complementary in situ measurements of microscopic heat transfer (**Figure 8c2**), coupled with controlled light irradiation, are also required [130,133].

These combined characterization techniques will reveal how localized photothermal heating dynamically regulates the ice-freezing pathway and interfacial lubrication behavior. Moreover, they will establish a quantitative structure-activity relationship among photothermal signal characteristics, lubricating film thickness, and ice adhesion performance.

5.4. Performance Evaluation Standards

Future research should prioritize developing a standardized performance evaluation system aligned with tribological lubrication standards to bridge the gap between laboratory validation and real-world engineering applications. Currently, most studies rely on lab-scale icing tests with inconsistent conditions, which hinders fair comparison across different material systems and impedes industrial translation.

 doi:10.20944/preprints202604.1367.v1

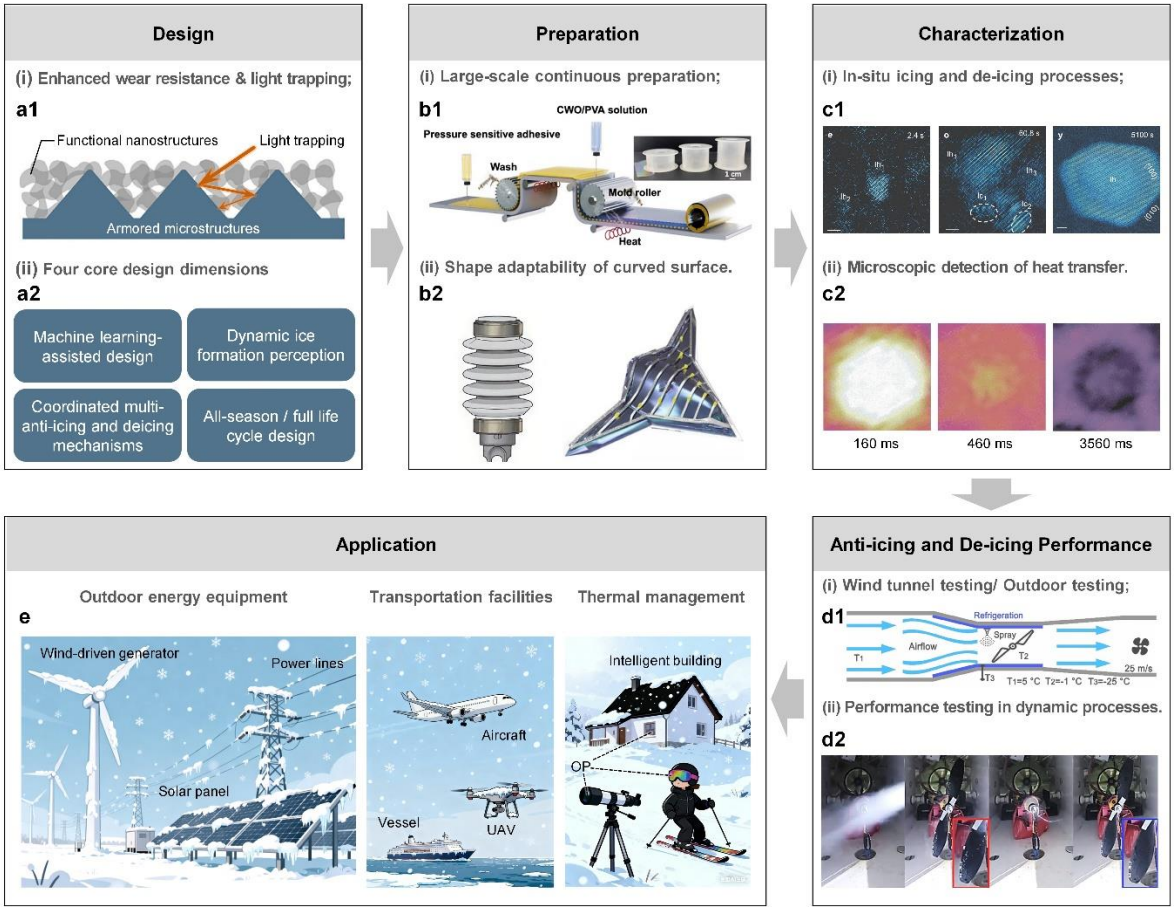

Figure 8. Future perspectives and outstanding challenges. (**a1**) The schematic design principle of the armored superhydrophobic ceramic surface. Reproduced with permission [127]. (**a2**) Four core dimensions for future material design. (**b1**) Scalable preparation of robust MXene films. Reproduced with permission [5]. (**b2**) Electrical insulators (left) and aircraft (right) with complex curved surface structures. Reproduced with permission [127,128]. (**c1**) Heterogeneous ice nucleation and growth processes under low temperature and low-pressure conditions. Reproduced with permission [129]. (**c2**) Thermographic images showing the halo pattern evolution and the heat transfer landscape during the freezing of a supercooled water drop. Reproduced with permission [130]. (**d1**) Schematic diagram of the open wind tunnel. Reproduced with permission [131]. (**d2**) Icing of the leading edge of the propeller with leading edge wrap in the wind tunnel operation. Reproduced with permission [131]. (**e**) Applications of photothermal anti-/de-icing materials.

The implementation path covers three core dimensions: (1) dedicated wind tunnel tests combining controllable icing clouds with tunable solar radiation (**Figure 8d1**) [1,131]; (2) long-term outdoor exposure tests across different climatic zones to obtain real-service performance data [26,90]; and (3) multi-field coupled dynamic fatigue tests to accelerate the evaluation of long-term material performance under dynamic service conditions (**Figure 8d2**) [124,131]. Core evaluation indicators should focus on maintaining interfacial water-film lubrication performance throughout the entire service cycle and on the tribological properties of the ice–substrate interface under actual operating conditions.

5.5. Toward Practical Applications

The industrial deployment of photothermal superhydrophobic anti-icing materials requires a critical shift from lab-scale efficacy validation toward robust, system-level engineering, centered on stabilizing the interfacial lubricating water film under real-world service conditions. As depicted in **Figure 8e**, these materials should be well-suited to complex dynamic environments, including core

 doi:10.20944/preprints202604.1367.v1

industrial scenarios (e.g., wind turbines, photovoltaic panels, transmission lines, aircraft) and civil applications (e.g., buildings, automotive windows, optical devices) [2,4–6,118,119,134].

To accelerate practical adoption, future research should focus on three priorities: (1) enhancing full-life-cycle environmental stability against UV degradation, chemical corrosion, and thermal cycling; (2) balancing high performance with low-cost, large-area manufacturing; and (3) developing scenario-adaptive system integration and intelligent control for on-demand, low-energy operation.

6. Conclusions

Photothermal-responsive superwetting surfaces based on the "water as a lubricating layer" strategy represent a paradigm shift in anti-icing/deicing technology and interfacial lubrication engineering. By converting solar energy into localized interfacial heat, these surfaces enable in situ formation of a continuous lubricating water film at the ice-substrate interface, transforming high-adhesion solid-solid contact into low-friction solid-liquid-solid lubrication. This intrinsic mechanism drastically reduces ice adhesion, enabling low-energy, high-efficiency full-cycle ice protection, while overcoming the bottlenecks of conventional SHS (external-force-dependent ice detachment) and slippery liquid-infused surfaces (irreversible lubricant depletion).

Significant progress has been made in developing high-efficiency photothermal materials, hierarchical micro-/nanostructures, and multifunctional systems, achieving notable anti-icing/deicing performance under laboratory conditions. However, critical bottlenecks remain for industrial translation: (1) the quantitative relationship between water film formation and lubrication failure is still unclear; (2) mechanical durability and service stability are inadequate; (3) all-weather adaptability of purely photothermal systems is limited; (4) systematic field validation and standardized evaluation protocols are lacking.

Future breakthroughs should focus on: (1) multi-dimensional material design; (2) scalable, conformal, and low-cost fabrication; (3) advanced in situ characterization of interfacial lubrication; (4) standardized performance evaluation; (5) scenario-optimized system integration. With continued progress, this technology is expected to enable large-scale applications in aerospace, power transmission, transportation, building energy efficiency, and optical devices, providing sustainable solutions to ice-accumulation hazards in extreme environments.

Author Contributions: Conceptualization, C.G.; writing---original draft preparation, C.G.; writing---review and editing, C.G., Y.L., Y. D.; supervision, C.G. Y.L.; funding acquisition, C.G. All authors have read and agreed to the published version of the manuscript.

Funding: This work was supported by the General Research Project of the Zhejiang Provincial Department of Education (Grant No. Y202558549), the Taizhou Municipal Science and Technology Project (Grant No. 25gya18), and the High-level Talent Introduction Research Initiation Grant Program of Taizhou Institute of Vocational Technology (Grant No. 2025GCC04).

Conflicts of Interest: The authors declare no conflicts of interest.

Abbreviations

The following abbreviations are used in this manuscript:

SHS	Superhydrophobic Surface
SLIPS	Slippery Liquid-Infused Porous Surface
LSPR	Localized Surface Plasmon Resonance
NIR	Near-Infrared
JDOS	Joint Density of States
CNT	Carbon Nanotube
PDMS	Polydimethylsiloxane
PCM	Phase Change Material

 doi:10.20944/preprints202604.1367.v1

References

1. Wang, X.; Zhang, Y.; Wang, J.; Li, K.; Xu, Z.; He, Q., Current research status of dynamic de-icing technology for propellers. *Adv. Colloid Interface Sci*. **2025**, 344.
2. Wang, Y.; Liao, Z.; Zeng, Q.; Li, G.; He, Y.; Yang, Y.; Song, Y.; Wang, L.; Liu, S.; Xuan, S., Robust and Energy-Effective Electrothermal Superhydrophobic Film with Micro-Hexagonal Groove Array Structure for Anti/Deicing. *Adv. Funct. Mater.* **2025**, e14771.
3. Li, Y.; Ma, W.; Kwon, Y. S.; Li, W.; Yao, S.; Huang, B., Solar Deicing Nanocoatings Adaptive to Overhead Power Lines. *Adv. Funct. Mater.* **2022**, 32, (25).
4. Zhou, M.; Zhang, L.; Zhong, L.; Chen, M.; Zhu, L.; Zhang, T.; Han, X.; Hou, Y.; Zheng, Y., Robust Photothermal Icephobic Surface with Mechanical Durability of Multi-Bioinspired Structures. *Adv. Mater.* **2023**, 36, (3).
5. Hao, T.; Zhang, P.; Chi, C.; Wang, Y.; Zhang, W.; Chen, X.; Wang, D.; Chen, X.; Ye, J.; Chen, W.; Kang, F.; Bai, Y.; Chen, Q.; Zhu, C.; He, Z., Transparent Anti-Icing Moiré-Film Enhancing Photovoltaic Stability in Extreme Cold Climates.*Adv. Mater.* **2025**.
6. Guo, Y.; Zhao, H.; Zhang, C.; Zhao, G., Super photothermal/electrothermal response and anti-icing/deicing capability of superhydrophobic multi-walled carbon nanotubes/epoxy coating. *Chem. Eng. J.* **2024**, 497.
7. Muthumani, A.; Fay, L.; Akin, M.; Wang, S.; Gong, J.; Shi, X., Correlating lab and field tests for evaluation of deicing and anti-icing chemicals: A review of potential approaches. *Cold Reg. Sci. Technol.* **2014**, 97, 21-32.
8. Rekuviene, R.; Saeidiharzand, S.; Mažeika, L.; Samaitis, V.; Jankauskas, A.; Sadaghiani, A. K.; Gharib, G.; Muganlı, Z.; Koşar, A review on passive and active anti-icing and de-icing technologies. *Appl. Therm. Eng.* **2024**, 250, 123474.
9. Okulov, V.; Kabardin, I.; Mukhin, D.; Stepanov, K.; Okulova, N., Physical de-icing techniques for wind turbine blades. *Energies* **2021**, 14, (20), 6750.
10. Li, Q.; Yao, R.; Tan, V. B. C.; He, F.; Zhao, H.; Bai, T., A review of efficient thermal application for ice detection and anti/de-icing technology. *Appl. Therm. Eng*. **2025**, 263.
11. Boinovich, L. B.; Emelyanenko, K. A.; Emelyanenko, A. M., Superhydrophobic versus SLIPS: Temperature dependence and the stability of ice adhesion strength. *J. Colloid Interface Sci.* **2022**, 606, (Part1).
12. Kreder, M. J.; Alvarenga, J.; Kim, P.; Aizenberg, J., Design of anti-icing surfaces: smooth, textured or slippery? *Nat. Rev. Mater.* **2016**, 1, (1).
13. Boreyko, J. B.; Chen, C.-H., Self-Propelled Dropwise Condensate on Superhydrophobic Surfaces. *Phys. Rev. Lett.* **2009**, 103, (18).
14. Cao, L.; Jones, A. K.; Sikka, V. K.; Wu, J.; Gao, D., Anti-Icing Superhydrophobic Coatings. *Langmuir* **2009**, 25, (21), 12444-12448.
15. Mishchenko, L.; Hatton, B.; Bahadur, V.; Taylor, J. A.; Krupenkin, T.; Aizenberg, J., Design of ice-free nanostructured surfaces based on repulsion of impacting water droplets. *ACS Nano* **2010**, 4, (12), 7699-7707.
16. Guo, P.; Zheng, Y.; Wen, M.; Song, C.; Lin, Y.; Jiang, L., Icephobic/Anti-Icing Properties of Micro/Nanostructured Surfaces. *Adv. Mater.* **2012**, 24, (19), 2642-2648.
17. Bird, J. C.; Dhiman, R.; Kwon, H.-M.; Varanasi, K. K., Reducing the contact time of a bouncing drop. *Nature* **2013**, 503, (7476), 385-388.
18. Liu, Y.; Moevius, L.; Xu, X.; Qian, T.; Yeomans, J. M.; Wang, Z., Pancake bouncing on superhydrophobic surfaces. *Nat. Phys.* **2014**, 10, (7), 515-519.
19. Papadopoulos, P.; Mammen, L.; Deng, X.; Vollmer, D.; Butt, H.-J. J. P. o. t. N. A. o. S. o. t. U. S. o. A., How superhydrophobicity breaks down. *PNAS* **2013**, 110, (9), 3254-3258.
20. Yang, C.; Sun, S.; Cheng, X.; Xie, S.; Guo, Z., Dynamic Icing Behavior of Icephobic Interfaces Under High-Humidity, High-Wind, and Low-Temperature Conditions. *Adv. Funct. Mater.* **2026**.
21. Golovin, K.; Dhyani, A.; Thouless, M. D.; Tuteja, A., Low–interfacial toughness materials for effective large-scale deicing. *Science* **2019**, 364, (6438), 371-375.
22. Wong, T.-S.; Kang, S. H.; Tang, S. K. Y.; Smythe, E. J.; Hatton, B. D.; Grinthal, A.; Aizenberg, J., Bioinspired self-repairing slippery surfaces with pressure-stable omniphobicity. *Nature* **2011**, 477, (7365), 443-447.

 doi:10.20944/preprints202604.1367.v1

23. Kim, P.; Wong, T. S.; Alvarenga, J.; Kreder, M. J.; Adorno-Martinez, W. E.; Aizenberg, J., Liquid-Infused Nanostructured Surfaces with Extreme Anti-Ice and Anti-Frost Performance. *ACS Nano* **2012**, 6, (8), 6569-6577.
24. Golovin, K.; Kobaku, S. P. R.; Lee, D. H.; Diloreto, E. T.; Mabry, J. M.; Tuteja, A., Designing durable icephobic surfaces. Sci. Adv. **2016**, 2, (3), e1501496.
25. Wang, D.; Sun, Q.; Hokkanen, M. J.; Zhang, C.; Lin, F.-Y.; Liu, Q.; Zhu, S.-P.; Zhou, T.; Chang, Q.; He, B.; Zhou, Q.; Chen, L.; Wang, Z.; Ras, R. H. A.; Deng, X., Design of robust superhydrophobic surfaces. Nature **2020**, 582, (7810), 55-59.
26. Dash, S.; de Ruiter, J.; Varanasi, K. K., Photothermal trap utilizing solar illumination for ice mitigation. Sci. Adv. **2018**, 4, (8), eaat0127.
27. Wu, S.; Du, Y.; Alsaid, Y.; Wu, D.; Hua, M.; Yan, Y.; Yao, B.; Ma, Y.; Zhu, X.; He, X., Superhydrophobic photothermal icephobic surfaces based on candle soot. *PNAS* **2020**, 117, (21), 11240-11246.
28. Zhang, H.; Zhao, G.; Wu, S.; Alsaid, Y.; Zhao, W.; Yan, X.; Liu, L.; Zou, G.; Lv, J.; He, X.; He, Z.; Wang, J., Solar anti-icing surface with enhanced condensate self-removing at extreme environmental conditions. *PNAS* **2021**, 118, (18).
29. Yang, S.; Liu, J.; Hoque, M. J.; Huang, A.; Chen, Y.; Yang, W.; Feng, J.; Miljkovic, N., A Critical Perspective on Photothermal De-Icing. *Adv. Mater.* **2024**, 37, (7).
30. Sheng, S.; Zhu, Z.; Wang, Z.; Hao, T.; He, Z.; Wang, J., Bioinspired solar anti-icing/de-icing surfaces based on phase-change materials. *Sci. China Mater.* **2021**, 65, (5), 1369-1376.
31. Haechler, I.; Ferru, N.; Schnoering, G.; Mitridis, E.; Schutzius, T. M.; Poulikakos, D., Transparent sunlight-activated antifogging metamaterials. *Nat. Nanotechnol.* **2022**, 18, (2), 137-144.
32. Mao, M.; Wei, J.; Li, B.; Li, L.; Huang, X.; Zhang, J., Scalable robust photothermal superhydrophobic coatings for efficient anti-icing and de-icing in simulated/real environments. *Nat. Commun.* **2024**, 15, (1).
33. Xu, H.; Lu, H.; Wang, J. X.; Luo, P.; Yu, F.; Feng, J.; Zhou, T., Full Life Cycle Deicing and Efficient Anti-Icing Surface on Polymers with Triple Thermal Conversion Capability. *Adv. Mater.* **2025**.
34. Du, J.; Wang, W.; Fu, Y.; Li, X.; Tan, J.; Li, H.; Chen, X.; Chu, F.; Min, Q.; Tso, C. Y., A self-regulated photothermal anti-/deicing film for all-season applications. *Nat. Commun.* **2026**.
35. Chu, F.; Hu, Z.; Feng, Y.; Lai, N. C.; Wu, X.; Wang, R., Advanced Anti-Icing Strategies and Technologies by Macrostructured Photothermal Storage Superhydrophobic Surfaces. *Adv. Mater.* **2024**, 36, (31).
36. Zhang, F.; Yao, B.; Song, M.; Chen, M., Transparent Solar Thermal Metasurface for Efficient Anti-Icing/Deicing and Indoor Light Management. *Adv. Funct. Mater.* **2025**, 2501463.
37. Yang, S.; Li, Q.; Du, B.; Ying, Y.; Zeng, Y.; Jin, Y.; Qin, X.; Gao, S.; Wang, S.; Wang, Z.; Wen, R.; Ma, X., Photothermal superhydrophobic copper nanowire assemblies: fabrication and deicing/defrosting applications. *Int. J. Extreme Manuf.* **2023**, 5, (4).
38. Hou, M.; Jiang, Z.; Zhang, X.; Sun, W.; Chu, F.; Lai, N.-C., Fabrication of hydrophobic photothermal phase change microcapsules for efficient anti-/deicing. *Mater. Today Chem.* **2024**, 40.
39. Hou, M.; Jiang, Z.; Sun, W.; Chen, Z.; Chu, F.; Lai, N. C., Efficient Photothermal Anti-/Deicing Enabled by 3D Cu2-xS Encapsulated Phase Change Materials Mixed Superhydrophobic Coatings. *Adv. Mater.* **2023**, 36, (3).
40. Li, Y.; Lin, C.; Wu, Z.; Chen, Z.; Chi, C.; Cao, F.; Mei, D.; Yan, H.; Tso, C. Y.; Chao, C. Y. H.; Huang, B., Solution-Processed All-Ceramic Plasmonic Metamaterials for Efficient Solar–Thermal Conversion over 100–727 °C. *Adv. Mater.* **2020**, 33, (1).
41. Ma, W.; Li, Y.; Chao, C. Y. H.; Tso, C. Y.; Huang, B.; Li, W.; Yao, S., Solar-assisted icephobicity down to −60°C with superhydrophobic selective surfaces. *Cell Rep. Phys. Sci.* **2021**, 2, (3).
42. Zhang, C.; Lei, Y.; Wang, K.; Jiang, B.; Ye, G.; Yuan, Y.; Sun, K.; Chen, Q.; Liu, T., Durable fluorine-free multilayer superhydrophobic coatings for synergistic photothermal and electrothermal anti-icing protection. *Prog. Org. Coat.* **2025**, 208, 109433.
43. Zhang, F.; Yan, H.; Chen, M., Multi-Scale Superhydrophobic Surface with Excellent Stability and Solar-Thermal Performance for Highly Efficient Anti-Icing and Deicing. *Small* **2024**, 20, (32).
44. Zhang, L.; Feng, Y.; Cao, X.; Dong, Y.; Liu, W.; Li, B.; Li, J.; Hao, C., Hierarchical Icephobic Surfaces with Enhanced Photothermal Performance for Sustainable Anti-Icing. *Adv. Sci.* **2025**, 12, (27).

 doi:10.20944/preprints202604.1367.v1

45. Hao, T.; Wang, D.; Chen, X.; Jazzar, A.; Shi, P.; Li, C.; Wang, H.; He, X.; He, Z., Photothermal strategies for ice accretion prevention and ice removal. *Appl. Phys. Rev.* **2023**, 10, (2).
46. Gao, C.; Wang, L.; Lin, Y.; Li, J.; Liu, Y.; Li, X.; Feng, S.; Zheng, Y., Droplets Manipulated on Photothermal Organogel Surfaces. *Adv. Funct. Mater.* **2018**, 28, (35).
47. Wu, D.; Ma, L.; Zhang, F.; Qian, H.; Minhas, B.; Yang, Y.; Han, X.; Zhang, D., Durable deicing lubricant-infused surface with photothermally switchable hydrophobic/slippery property. *Mater. Des.* **2020**, 185.
48. Yang, X.; Liu, Y.; Zhong, Y.; Chen, H., Ultra-durable photothermal anti-/de-icing superhydrophobic coating with water droplets freezing from the outside in. *J. Colloid Interface Sci.* **2025**, 682, 1127-1139.
49. Zhang, L.; Gao, C.; Zhong, L.; Zhu, L.; Chen, H.; Hou, Y.; Zheng, Y., Robust photothermal superhydrophobic coatings with dual-size micro/nano structure enhance anti-/de-icing and chemical resistance properties. *Chem. Eng. J.* **2022**, 446, 137461.
50. Li, W.; Wang, T.; Feng, H.; Cheng, J.; Lin, C.; Wang, X.; Wang, W.; Chen, S., Robust photothermal self-healing superhydrophobic composite coating for durable anti/de-icing applications. *Chem. Eng. J.* **2025**, 505, 159218.
51. Wu, Y.; Dong, L.; Shu, X.; Zhang, Y.; Ran, Q., Breathable and self-healing photothermal superhydrophobic coating featuring exceptional liquid impalement resistance and anti-/deicing capabilities for concrete materials. *ACS Appl. Mater. Interfaces* **2025**, 17, (12), 18852-18868.
52. Tao, J.; Wu, H.; Xie, J.; Lu, Z.; Li, S.; Jin, M.; Zhao, H.; Dong, L.; Chen, S.; Yang, Y., Mechanically Interlocked Bioinspired Armor: Sea Urchin-Mimetic Superhydrophobic Coatings with Ultrahigh Durability for Anti-Icing/Deicing. *Small* **2025**, 2505827.
53. Zhang, Q.; Chen, Y.; Liu, R.; Luo, J., Efficiently all-weather anti-icing and de-icing coatings enabled by polyaniline microcapsules encapsulated phase change materials. *Chem. Eng. J.* **2024**, 499.
54. Liu, Q.; Wang, Y.; Liu, X.; Li, Y.; Yu, E.; Sun, Z.; Wang, L.; Zhuang, G.; Yu, J.; Liu, S., Robust and Ultra-Efficient Anti-/De-Icing Surface Engineered Through Photo-/Electrothermal Micro-Nanostructures With Switchable Solid-Liquid States. *Adv. Mater.* **2024**, 37, (5).
55. Sun, R. Y.; Wang, F.; Tan, Y.; Li, J. L.; Jiang, Z. S.; Deng, C.; Song, F.; Wang, Y. Z., Breathable Nanorod-Embedded Hierarchical Photothermal Coatings with Anti-Soiling and Safe Thermal Regulation for Efficient Anti-Icing and De-Icing. *Small* **2025**.
56. Wu, S.; Liang, Z.; Li, Y.; Chay, S.; He, Z.; Tan, S.; Wang, J.; Zhu, X.; He, X., Transparent, Photothermal, and Icephobic Surfaces via Layer-by-Layer Assembly. *Adv. Sci.* **2022**, 9, (14).
57. Zhang, R.; Zhang, H.; Dong, S.; Yang, Y.; Li, J., Photo- and Electro-Responsive Super-Slippery Oleogel Coating for Ultra-Low Temperature Ice-Phobic Applications. *Adv. Funct. Mater.* **2025**.
58. Yang, B.; Zhang, Z.; Liu, P.; Fu, X.; Wang, J.; Cao, Y.; Tang, R.; Du, X.; Chen, W.; Li, S., Flatband λ-Ti3O5 towards extraordinary solar steam generation. *Nature* **2023**, 622, (7983), 499-506.
59. Cao, Z.; Gong, Z.; Ma, X.; Peng, J.; Xiong, Y.; Nie, Y.; Duan, Y.; Li, H.; Zhou, S.; Rao, T.; Chen, Q.; Wang, P., A superhydrophobic/photothermal synergistic anti-icing mesh with active/passive anti-icing function. *Mater. Res. Express* **2024**, 11, (7).
60. Jamil, M. I.; Wang, Q.; Ali, A.; Hussain, M.; Aziz, T.; Zhan, X.; Zhang, Q., Slippery Photothermal Trap for Outstanding Deicing Surfaces. *J. Bionic Eng.* **2021**, 18, (3), 548-558.
61. Qian, C.; Wang, L.; Li, Q.; Chen, X., A Strategy of Candle Soot-Based Photothermal Icephobic Superhydrophobic Surface. *Coatings* **2024**, 14, (5).
62. Xia, X.; Chen, H.; Wang, Y.; Yu, H.; Zou, B.; Zhang, Y., Robust Stick-and-Play Photothermal Icephobic Film with Bioinspired Insulation Cells. *Adv. Sci.* **2025**, 12, (18).
63. Zhao, Y.; Li, Q.; Liu, Z.; Alsaid, Y.; Shi, P.; Jawed, M. K.; He, X., Sunlight-powered self-excited oscillators for sustainable autonomous soft robotics. *Sci. Robot.* **2023**, 8, (77).
64. Xu, S.; Huang, X.; Sheng, H.; Wang, X.; Hu, W.; Ji, Z.; Liu, H., Advanced Slippery Coatings Featuring Ternary Photothermal Traps for Superior Anti/De-Icing and Anti/De-Frosting Efficiency in Extreme Dynamic Cold Environment. *Adv. Funct. Mater.* **2025**.
65. Chen, C.; Guo, S.; Zhang, L.; Yao, H.; Liu, B.; Zhang, C.; Zhang, Y.; Lao, Z.; Wu, S.; Wu, D., Multifunctional shape-memory smart window based on femtosecond-laser-printed photothermal microwalls. *Int. J. Extreme Manuf.* **2024**, 7, (1), 015504.

 doi:10.20944/preprints202604.1367.v1

66. Wei, J.; Liang, W.; Mao, M.; Li, B.; Zhang, J., Facile Preparation of Impalement Resistant, Mechanically Robust and Weather Resistant Photothermal Superhydrophobic Coatings for Anti-/De-icing. *Chem. Asian J.* **2024**, 19, (9).
67. Zarasvand, K. A.; Nazemi, A.; Lahiri, S. K.; Tetreault, A.; Milani, A. S.; Bender, T. P.; Golovin, K., Skin-Inspired Nanofluid-Filled Surfaces with Tunable Icephobic, Photothermal, and Energy Absorption Properties. *Adv. Funct. Mater.* **2023**, 33, (46).
68. Tan, S.; Han, X.; Cheng, S.; Guo, P.; Wang, X.; Che, P.; Jin, R.; Jiang, L.; Heng, L., Photothermal Solid Slippery Surfaces with Rapid Self-Healing, Improved Anti/De-Icing and Excellent Stability. *Macromol. Rapid Commun.* **2023**, 44, (6).
69. Wang, L.; Zhang, C.; Zhang, Y.; Shen, C.; Xin, Z.; Wei, Z., Bionic Fluorine-Free Multifunctional Photothermal Surface for Anti/de/Driving-Icing and Droplet Manipulation. *Adv. Sci.* **2024**, 11, (46).
70. Yang, C.; Guo, Z., Biomimetic Xanthium Strumarium Inspired Superhydrophobic Anti-/De-Icing Films with Near-Infrared Light-Induced Self-Healing. *Small* **2025**, 21, (26).
71. Yang, H.; Wang, Z.; Tan, S.; Zang, R.; Li, C.; He, Z.; Meng, J.; Wang, S.; Wang, J., Bio-Inspired Anti-Icing Material as an Energy-Saving Design toward Sustainable Ice Repellency. *Adv. Mater. Technol.* **2022**, 7, (12).
72. Zhang, N.; Kong, X.; Chang, Y.; Qiao, W.; Zhang, M.; Kang, R., Robust photothermal superhydrophobic concrete coating for efficient anti-icing/de-icing. *J. Build. Eng.* **2025**, 101, 111842.
73. Wei, Y.; Zhang, J.; Huang, Z.; Yu, Q.; Liang, G.; Rao, L.; Chao, X.; Li, J.; Wu, J.; Yu, S., Laser-scribed wood photoabsorbers for sustainable interfacial solar steam and electricity co-generation. *Energy Convers. Manag.* **2025**, 344, 120291.
74. Ji, H.; Yang, C.; Su, H.; Qi, Z.; Wang, Y.; Cheng, E.; Hu, N., Multifunctional superhydrophobic film with comprehensive icing monitoring, anti-icing, and photothermal/electrothermal deicing properties. *Prog. Org. Coat.* **2025**, 206, 109337.
75. Li, R.; Tian, S.; Tian, Y.; Wang, J.; Xu, S.; Yang, K.; Yang, J.; Zhang, L., An Extreme-Environment-Resistant Self-Healing Anti-Icing Coating. *Small* **2022**, 19, (10).
76. Yin, T.; Gao, H.; Zhou, Y.; Du, Y.; Jin, H.; Wen, D., A superhydrophobic SiO2/rGO composite coating with enhanced photothermal properties for anti-icing/deicing. *J. Mater. Chem. C* **2025**, 13, (32), 16607-16619.
77. Zhu, X.; Liu, J.; Zhao, W.; Yu, W.; Liu, X., Design of phase change composite with hierarchical energy-transfer pathway via laser-induced graphene for efficient energy storage, conversion, and utilization. *Chem. Eng. J.* **2023**, 460.
78. Zhang, L.; Luo, B.; Fu, K.; Gao, C.; Han, X.; Zhou, M.; Zhang, T.; Zhong, L.; Hou, Y.; Zheng, Y., Highly efficient photothermal icephobic/de-icing MOF-based micro and nanostructured surface. *Adv. Sci.* **2023**, 10, (34), 2304187.
79. Song, S.; Liu, Y., Mechanochemically durable superhydrophobic photothermal responsive coating toward effectively anti-corrosion and anti-icing/deicing. *Constr. Build. Mater.* **2025**, 482, 141639.
80. Zhao, B.; Shi, X.; Khakalo, S.; Meng, Y.; Miettinen, A.; Turpeinen, T.; Mi, S.; Sun, Z.; Khakalo, A.; Rojas, O. J.; Mattos, B. D., Wood-based superblack. *Nat. Commun.* **2023**, 14, (1).
81. Xu, R.; Cui, H.; Wei, N.; Yu, Y.; Dai, L.; Chen, X., Biomimetic Micro-Nanostructured Evaporator with Dual-Transition-Metal MXene for Efficient Solar Steam Generation and Multifunctional Salt Harvesting. *Nano-Micro Lett.* **2025**, 17, (1).
82. Li, X.; Liu, Y.; Zhang, Z.; Liu, Y.; Leng, J., Icephobic materials and strategies: From bio-inspirations to smart systems. *Droplet* **2024**, 3, (3).
83. Ross, M. B.; Blaber, M. G.; Schatz, G. C., Using nanoscale and mesoscale anisotropy to engineer the optical response of three-dimensional plasmonic metamaterials. *Nat. Commun.* **2014**, 5, (1).
84. Xia, X.; Xia, Y., Gold nanocages as multifunctional materials for nanomedicine. *Front. Phys.* 2013, 9, (3), 378-384.
85. Zhou, L.; Tan, Y.; Ji, D.; Zhu, B.; Zhang, P.; Xu, J.; Gan, Q.; Yu, Z.; Zhu, J., Self-assembly of highly efficient, broadband plasmonic absorbers for solar steam generation. *Sci. Adv.* **2016**, 2, (4), e1501227.
86. Liu, N.; Schneider, C.; Freitag, D.; Hartmann, M.; Venkatesan, U.; Müller, J.; Spiecker, E.; Schmuki, P., Black TiO2 Nanotubes: Cocatalyst-Free Open-Circuit Hydrogen Generation. *Nano Lett.* **2014**, 14, (6), 3309-3313.

 doi:10.20944/preprints202604.1367.v1

87. Zhou, W.; Li, W.; Wang, J.-Q.; Qu, Y.; Yang, Y.; Xie, Y.; Zhang, K.; Wang, L.; Fu, H.; Zhao, D., Ordered Mesoporous Black TiO2 as Highly Efficient Hydrogen Evolution Photocatalyst. *J. Am. Chem. Soc.* **2014**, 136, (26), 9280-9283.
88. Wang, B.; Wang, C.; Li, Y.; Jin, J.; Lin, X.; Shi, C., Bionic design: insights from nature for solar interfacial evaporators. *Energy Environ. Sci.* **2025**, 18, (8), 3432-3461.
89. Wu, X.; Wang, Y.; Li, J.; Wang, W.; Cheng, X.; Li, C.; Zhao, Z. Y.; Liu, Y.; Liu, X. Q., Durable and Ultra-Black Superhydrophobic Coatings for High-Efficiency Photothermal Applications Under Harsh Conditions. *Adv. Optical Mater.* **2026**, 14.
90. Zhou, M.; Zhang, T.; Wei, H.; Zhu, L.; Gao, C.; Luo, Q.; Hou, Y.; Zheng, Y., Mosquito-Eye-Inspired Photothermal Icephobic Surface with Enhanced Anti-Icing and Deicing Efficiency. *ACS Appl. Mater. Interfaces* **2025**, 17, (25), 37300-37310.
91. Miljkovic, N.; Enright, R.; Nam, Y.; Lopez, K.; Dou, N.; Sack, J.; Wang, E. N., Jumping-Droplet-Enhanced Condensation on Scalable Superhydrophobic Nanostructured Surfaces. *Nano Lett.* **2012**, 13, (1), 179-187.
92. Wang, L.; Li, D.; Jiang, G.; Hu, X.; Peng, R.; Song, Z.; Zhang, H.; Fan, P.; Zhong, M., Dual-Energy-Barrier Stable Superhydrophobic Structures for Long Icing Delay. *ACS Nano* **2024**, 18, (19), 12489-12502.
93. Wang, L.; Tian, Z.; Jiang, G.; Luo, X.; Chen, C.; Hu, X.; Zhang, H.; Zhong, M., Spontaneous dewetting transitions of droplets during icing & melting cycle. *Nat. Commun.* **2022**, 13, (1).
94. Li, D.; Zhang, Y.; Gao, S.; Wang, Z.; Bai, G., Transparent Anti-Icing Coating via Synergistic Nanoscale Interfacial Engineering and Spectral-Selective Photothermy. *Adv. Funct. Mater.* **2025**.
95. Xie, Z.; Wang, H.; Geng, Y.; Li, M.; Deng, Q.; Tian, Y.; Chen, R.; Zhu, X.; Liao, Q., Carbon-Based Photothermal Superhydrophobic Materials with Hierarchical Structure Enhances the Anti-Icing and Photothermal Deicing Properties. *ACS Appl. Mater. Interfaces* **2021**, 13, (40), 48308-48321.
96. Liu, J.; Zhu, C.; Liu, K.; Jiang, Y.; Song, Y.; Francisco, J. S.; Zeng, X. C.; Wang, J., Distinct ice patterns on solid surfaces with various wettabilities. *PNAS* **2017**, 114, (43), 11285-11290.
97. Xue, Y.; Verdross, P.; Liang, W.; Woodward, R. T.; Bismarck, A., Breaking the ice: Applications of photothermal superhydrophobic materials for efficient deicing strategies. *Adv. Colloid Interface Sci.* **2025**, 103489.
98. Zhang, W.; Wang, D.; Sun, Z.; Song, J.; Deng, X., Robust superhydrophobicity: mechanisms and strategies. Chemical Society Reviews **2021**, 50, (6), 4031-4061.
99. Chen, M., Sandpaper-Inspired Scalable and Robust Solar Thermal Superhydrophobic Surface for Durable Anti-Icing/Deicing. *Adv. Funct. Mater.* **2026**.
100. Liu, J.; Pei, K.; Zhou, Y.; Fu, S.; Ai, S.; Wang, Y.; Jiang, H.; Zhou, Z.; Guo, Z., Bioinspired Ultrasmall-Bandgap MOF-Integrated Superhydrophobic Textiles via In Situ Self-Assembly: Enabling Next-Generation Multifunctional Smart Textiles. *Adv. Funct. Mater.* **2025**.
101. Lu, H.; Chen, L.; Sha, X.; Chen, G., Multi-functional superhydrophobic photothermal cotton fabric inspired by mussels with anti-icing/de-icing and oil-water separation functions. *Surf. Coat. Technol.* **2025**, 515.
102. Li, Q.; Yang, S.; Ying, Y.; Liu, Y.; Wen, R.; Miljkovic, N.; Ma, X., Scalable Photothermal Superhydrophobic Deicing Coating with Mechanochemical-Thermal Robustness. *ACS Appl. Mater. Interfaces* **2025**.
103. Peng, C.; Chen, Z.; Tiwari, M. K., All-organic superhydrophobic coatings with mechanochemical robustness and liquid impalement resistance. *Nat. Mater.* **2018**, 17, (4), 355-360.
104. Bai, X.; Chen, W.; Wang, P., Structural Self-Healing Superhydrophobic Surfaces: Healing Mechanisms, Methods, and Future Challenges. *Adv. Mater. Interfaces* **2025**.
105. Zhang, Y.; Xu, Y.; Wang, F.; Huang, W.; Lei, Y.; Li, X.; Sui, X.; Li, Z.; Chang, X., Photothermal self-adaptive PSF-TO/PPy@BN dual-functional epoxy coating: Photothermally enhanced anti-icing and self-healing. *Prog. Org. Coat.* **2025**, 209.
106. Zhang, Q.; Zhang, S.; Liu, R.; Luo, J., Near-Infrared Light-Responsive Lubricating Coating with Polyaniline Microspheres for Long-Term Anti-Icing and High-Efficiency De-Icing. *Small* **2025**.
107. Niu, W.; Chen, G. Y.; Xu, H.; Liu, X.; Sun, J., Highly Transparent and Self-Healable Solar Thermal Anti-/Deicing Surfaces: When Ultrathin MXene Multilayers Marry a Solid Slippery Self-Cleaning Coating. *Adv. Mater.* **2022**, 34, (10).

 doi:10.20944/preprints202604.1367.v1

108. Zhang, J.; Singh, V.; Kabi, P.; Huang, W.; Bahal, S.; Papakonstantinou, I.; Tiwari, M. K., Reticular photothermal traps enabling transparent coatings with exceptional all-day icephobicity. *Nano Today* **2025**, 62.
109. Gao, H.; Zhou, Y.; Ma, J.; Jin, H.; Bao, J.; Wen, D., Recent advancements in electro-thermal anti-/de-icing materials. *RSC Adv.* **2025**, 15, (22), 17102-17115.
110. Shi, J.; Ke, S.; Wang, F.; Wang, W.; Wang, C., Recent advances in photothermal anti-/de-icing materials. *Chem. Eng. J.* **2024**, 481.
111. Lin, C.; Ma, W.; Zhang, Y.; Law, M. K.; Li, C. Y.; Li, Y.; Chen, Z.; Li, K.; Li, M.; Zheng, J.; Fu, Y.; Yan, X.; Chi, C.; Yang, J.; Li, W.; Yao, S.; Huang, B., A Highly Transparent Photo-Electro-Thermal Film with Broadband Selectivity for All-Day Anti-/De-Icing. *Small* **2023**, 19, (40).
112. Li, G.; Wang, X.; Zhang, F.; Yin, L.; Zhang, D.; Zhao, K.; Zhang, Z.; Qian, X.; Jiang, Y.; Zhang, S., A hydrophobic electroless copper-nickel fabric with dual drive energy conversion for all-weather anti-icing/icephobic and deicing. *Surf. Interfaces* **2024**, 53.
113. Sun, L.; Gao, C.; Li, W., Programmable Control of Droplets on Phase-Change Lubricant-Infused Surfaces Under Low Voltage. *Lubricants* **2025**, 13, (6).
114. Sheng, S.; Zhang, Z.; Zhao, Z.; Ning, Y.; Yu, C.; Liu, K.; Jiang, L., Photo/Electro-Thermal Superhydrophobic Wood with Phase Change Materials for Highly Efficient Anti-/Deicing. *Adv. Funct. Mater.* **2025**, 35, (33).
115. Li, X.; Liu, Y.; Ma, Y.; Liu, H.; Wu, Y.; Zhou, F., Biomimetic Laminated Photothermal Superhydrophobic Energy-Storage Coatings with Synergistic Temperature-Matched Phase Change for Enhanced Anti-Icing and Deicing. *ACS Appl. Mater. Interfaces* **2025**.
116. Azimi Yancheshme, A.; Allahdini, A.; Maghsoudi, K.; Jafari, R.; Momen, G., Potential anti-icing applications of encapsulated phase change material–embedded coatings; a review. *J. Energy Storage* **2020**, 31.
117. Miao, S.; Sun, L.; Liu, X.; Chen, Y., Photo-Electro-Thermal Switchable Hydrophobic/Slippery Icephobic Surfaces Based on Multi-Wall Carbon Nanotubes for Passive Anti-Icing and Active Deicing. *Adv. Mater. Technologies* **2025**.
118. Han, X.; Xie, Y.; Sun, M.; Zhao, D.; Liu, K.; Heng, L.; Jiang, L., Transparent Photothermal Slippery Surface Based on Monolayer Self-Assembled MXene Film for Anti-Fogging and De-Icing. *Adv. Sci.* **2026**.
119. Zhang, W.; Zhang, J.; Wang, C.; Shi, J.; Wei, D.; Zhao, Z.; Wang, F., Color/Transparent Bi-Customizable Solar Antifogging Nanofilms. *Laser Photon. Rev.* **2024**, 19, (4).
120. Zhong, H.; Xiang, C.; Hu, Z.; Yang, X.; Liu, H.; Wang, R., Plasmonic photothermal superhydrophobic surface with nanotubes thermal insulating blanket for anti-icing and anti-frosting under weak light illumination. *Mater. Today Phys.* **2025**, 50.
121. Le, T. C.; Nguyen, D.-N.; Kaminski, D.; Kolver, T.; Subramanian, P.; Bateman, S., Harnessing Machine Learning for the Design of Surface Coatings: Challenges and Opportunities. *ACS Appl. Mater. Interfaces* **2025**, 17, (28), 39795-39808.
122. Fu, J.; Li, Y.; Song, X.; Liu, C.; Zhao, R.; Wang, H.; Wang, Q., Wettability prediction and feature importance analysis for laser-chemical induced superwetting surface based on machine learning. *J. Manuf. Process.* **2025**, 152, 57-67.
123. Zhao, L.; Shen, Y.; Tao, J.; Liu, W.; Wang, T.; Liu, S., Review on Icephobicity of Materials Surface Enhanced by Interface Action Force. *Adv. Mater. Interfaces* **2024**, 12, (6).
124. Yang, C.; Sun, S.; Cheng, X.; Xie, S.; Guo, Z., Dynamic Icing Behavior of Icephobic Interfaces Under High-Humidity, High-Wind, and Low-Temperature Conditions. *Adv. Funct. Mater.* **2026**, n/a, (n/a), e28597.
125. Yang, Q.; Yang, J.; Hu, Y.; Niu, X.; Liu, Z.; Zou, J.; Guo, J.; Xiong, H.; Gu, X.; Yang, L.; Yu, F.; Zhu, S.; Ye, M.; Yi, X.; Deng, X., A skin-inspired durable de-icing surface with boosting interfacial cracks. *Natl. Sci. Rev.* **2025**, 12, (3), nwaf005.
126. Xu, S.; Li, R.; Tian, S.; Yu, J.; An, C.; Yang, K.; Yang, J.; Zhang, L., Self-healing unmanned aerial vehicle skin for icing prevention and intelligent monitoring. *npj Flex. Electron.* **2025**, 9, (1).
127. Shao, H.; Luo, J.; Xue, P.; Shi, Z.; Sun, B.; Zhang, Y.; Zhou, Y.; Luo, Z.; Wang, P.; Wang, D.; Deng, X., Armored Superhydrophobic Ceramic Surfaces with Robust Weather Resistance. *Small* **2025**.

 doi:10.20944/preprints202604.1367.v1

128. Jiang, C.; Li, W.; Wu, Q.; Wang, Z.; Wang, K.; Pan, B.; Zong, H.; Li, X.; Liu, J.; Yuan, B.; Li, T.; Tian, X.; Huang, X.; Wang, H.; Guo, R., Shape-adaptive electronics based on liquid metal circuits printed on thermoplastic films. *Nat. Electron.* **2026**, 9, (1), 45-58.
129. Wang, Z.; Yuan, Z.; Cheng, M.; Huang, X.; Liu, K.; Wang, Y.; Sun, H.; Liao, L.; Xu, Z.; Chen, J.; Wang, W.; Liu, L.; Bai, X.; Xu, L.; Wang, E.; Wang, L., Molecularly resolved mapping of heterogeneous ice nucleation and crystallization pathways using in-situ cryo-TEM. *Nat. Commun.* **2025**, 16, (1).
130. Zhen, S.; Feng, H.; Lin, S.; Jin, Y.; Li, Z.; Deng, X.; Bonaccurso, E.; Chen, L., Condensate Halos in Condensation Frosting. *Adv. Sci.* **2025**, 12, (14).
131. Jia, Y.; Li, A.; Wang, J.; Wang, X.; Zhang, F.; Guo, Q.; He, Q., Durable Ceramicization-Induced Uncoated Superhydrophobic Surfaces for Anti-Icing Propeller Edges. *Adv. Mater.* **2025**, 37, (42).
132. Wan, S.; Chen, Y.; Huang, C.; Huang, Z.; Liang, C.; Deng, X.; Cheng, Q., Scalable ultrastrong MXene films with superior osteogenesis. *Nature* **2024**, 634, (8036), 1103-1110.
133. Schutzius, T. M.; Jung, S.; Maitra, T.; Graeber, G.; Köhme, M.; Poulikakos, D., Spontaneous droplet trampolining on rigid superhydrophobic surfaces. *Nature* **2015**, 527, (7576), 82-85.
134. Na, Z.; Liang, X.; Wang, H.; Yu, L.; Fan, C.; Wang, Q.; Wang, X.; Yang, H., Broadband Modulation, Self-Driven, and Self-Cleaning Smart Photovoltaic Windows for High Efficiency Energy Saving Buildings. *Adv. Funct. Mater.* **2023**, 34, (2).